Study on End Face Combustion Behavior of Highly Densified Biomass Briquette

(高密度バイオマスブリケットの端面燃焼に関する研究)

Hui YAN

Study on End Face Combustion Behavior of Highly Densified Biomass Briquette

By

Hui YAN

Submitted to the Department of Mechanical and Space Engineering, Hokkaido University, Japan, in Partial Fulfillment of the Requirement for the Degree of Doctor of Philosophy in Mechanical and Space Engineering

March 2017

Abstract

End-face combustion experiments and one-dimensional calculations were conducted on cylindrical bio-coke (BIC), i.e., a highly densified biomass briquette, to investigate whether quasi-one-dimensional steady combustion can be attained in forced air flow with different air temperature and air flow rate, as measured by a steady regression rate.

In the experiments with 300K air flow, the air flow rate was the main test and the results show that steady combustion of the BIC sample could be attained in 9.17NL/s or larger and, in contrast, extinction was observed in 7.50 NL/s or lower. In the calculation with 300K air flow condition, we obtained the mechanism that results in steady combustion and predicted the effect of BIC density and blowing on the extinction limit.

However, in the experiments with 400K air flow condition, it was found that the average regression rate in the first 0.01m of BIC was relatively small after ignition, whereas after the first 0.01m, the average regression rate became almost steady and much larger than that in the first 0.01m. This suggests that before the steady regression period is reached, a non-negligible unstable regression rate phase exists. We investigated this transient combustion phase by means of one-dimensional numerical calculations and the time-dependent regression rate and temperature distributions were computed. The mechanisms controlling transient combustion and the effects of different parameters on transient combustion behavior were examined. The results show that a transient combustion period exists before steady combustion is achieved. This transient combustion period decreases as volatile content increases, and moisture content has a similar effect on transient combustion as volatile content. A rising tendency of transient combustion period is observed with the increase Bio-coke density. Low air flow rate obtains long transient combustion period. Such phenomenon can be explained by the different final

steady temperature distribution and evolution rate from the initial temperature distribution to the final steady temperature distribution.

Finally, we investigated the effect air temperature on the transient combustion, results show the transient region becomes shorter but more evident as air temperature increases, which is due to remarkable increase of regression rate during the short transient period. That explains why we observe quasi-steady combustion with 300K air flow.

In Chapter 1, we show the definition of biomass fuel and summarize the studies of pyrolysis and combustion behaviors of solid biomass fuel. Then we introduce our newly developed biomass fuel, Bio-coke (BIC), and elucidate our previous researches about BIC. Finally, objective and scope of this study are presented.

In Chapter 2, we introduce the properties of Bio-coke in detail, including the feedstock of BIC, manufacture process of BIC, density, elemental analysis and proximate analysis of BIC.

In Chapter 3, the experimental setup (end-face combustion experimental setup) and procedure are described, as well as the one-dimensional numerical model. Then, based on the thermogravimetric analyses, the kinetic parameters of drying and pyrolysis reaction of Bio-coke are obtained by means of multi-component devolatilization mechanisms and one-component mechanisms of primary pyrolysis, respectively.

In Chapter 4, steady combustion of Bio-coke is discussed both in calculation and experiment. The combustion reaches a steady state in high air flow rate (9.17NL/s or larger), but extinction is observed in low air flow velocity (7.50 NL/s or lower), and effects of Bio-coke density and blowing on extinction limit are investigated.

In Chapter 5, end-face combustion in the transient period between ignition and steady combustion has been investigated. A one-dimensional numerical model is established to study

the change of regression rate and temperature distribution in BIC samples placed in opposed convective air flow and compared with experimental findings. Moreover, mechanisms for controlling the transient characteristics of BIC in end-face combustion and effects of the various parameters in the transient combustion stage are investigated.

In Chapter 6, conclusions are briefly summarized.

Keywords: Biomass briquette; Transient; Regression rate; Temperature distribution; Solid combustion; Extinction limit; Steady; Pyrolysis; Drying; Combustion

Thesis Supervisor: Osamu Fujita

Title: Professor

Acknowledgements

First and foremost, I would like to express my most sincere gratitude to my advisor, Prof. Osamu Fujita. He is the first teacher who took me to combustion field, he taught me the knowledge of combustion from the most fundamental level, block by block, brick by brick, without him, the door of combustion will always be close to me. He created fantastic research atmosphere for me, shared me lots of good ideas to improve my study during my Ph.D. course and encouraged me when I was struggling. What I learned from him is not only the knowledge of combustion but also the way to think scientifically and express logically. He also offered me lots of personal help during my Ph.D. period, I'll always appreciate that. He is a great scientist and even a better gentleman.

I would like to thank Prof. Harunori Nagata, Prof. Hideyuki Ogawa, Prof. Nozomu Hashimoto and Prof. Osamu Fujita for their services on my doctoral committee and also for their help on my study and research in the past years. I appreciate Prof. Takashi Nakamura, Prof. Nobuyuki Oshima, Prof. Kazuaki Sasaki, Prof. Masao Watanabe, Prof. Hiroshi Terashima, Prof. Katsuhiko Sasaki, Prof. Takemi Chikahisa and Prof. Koichi Sasaki on judgment committee.

I want to acknowledge my master-course advisor, Prof. Zhongming Xu (Chongqing University, China), for his continuous concern. He spent lots of effort on training me to be a good researcher during my master course and encouraged me to study aboard for Ph.D. program.

I would like to express my special appreciation to Prof. Yuji Nakamura for his generous help on my work, I learned lots of knowledge from him especially the numerical calculation skill. I also want to thank Ms. Miho Taga for her kind help for dealing a lot of paper works

related to my research and business trips.

I also wish to thank Dr. Akter Hossain, Dr. Jian Gao, Dr. Nepal Chandra Roy for the inspiring discussions with them. I appreciate Mr. Kenichi Sato, Mr. Yongho Chung, Mr. Hadi Bin Khalid, Mr. Guo Feng and Mr. Yushin Naito for their help for my life and research, I want to say thank you to all members in our laboratory as well as the former graduate students for their generous help that makes my life smooth here at HU.

I have met many good people at HU. It is hard to acknowledge all of them here. Some of them are Yanhua Lei, Xiaojing Sui, Qian Xiong, Huiying Cai, and Longhua Hu (USTC). I am grateful to them for their friendship and the parties enjoyed with them in the past years gave me warmness and happiness.

I want to acknowledge Ms. Ziyun Li, for the love and help.

My warmest appreciation to my friends, Dr. YangKyun Kim and Dr. SungHwan Youn, for the friendship we formed in Japan.

I wish to acknowledge China Scholarship Council (CSC) and Hokkaido University for providing me a scholarship for 42 months and 24 months of JASSO Honors Scholarship to pursue my study in Japan as a Ph.D. student.

Finally, with great humble and gratitude, I thank my parents, Xiaoming Yan and Zhiqiong Yang, for their endless love and concern. With their support, I am able to fully devote myself to my study.

Thanks to my daughter Yuman Yan

Table of Contents

Nomenclature

A	: frequency factor
c_p	: specific heat
ce	: cellulose
E	: activation energy
g	: gas
h	: enthalpy
H	: heat transfer coefficient
H_n	: heat transfer coefficient without blowing
H_d	: mass transfer coefficient
hc	: hemicellulose
l	: lignin
K	: reaction rate constant
M	: molecular weight
m	: mass
m''	: mass flux
n	: reaction order
Q	: reaction heat
R	: universal gas constant
r	: yield of fraction
rr	: regression rate
$rtol$	: criterion tolerance
S	: minimum coefficient in Levenberg-Marquardt nonlinear fitting algorithm
T	: temperature
t	: time
Y	: mass fraction
Δx	: grid size

Greek symbols

ω	: reaction rate
ε	: emissivity

λ : thermal conductivity

φ : stoichiometric coefficient

ρ : density

σ : Stefan–Boltzmann constant

θ : molecule weight ratio between oxygen and char

β : heating rate

δ : time scale

τ : ratio between co and co_2

Subscripts

air : air flow

am : ambient

ash : ash

B : bottom side of BIC

c : char

ce : cellulose

g : gas

hc : hemicellulose

ht : heat transfer

gi : grid

j : wet BIC, dry BIC, char and ash

l : lignin

O_2 : oxygen

onset : initiation

offset : tailing region in DTG

peak : maximum devolatilization rate

rr : regression rate

s : solid

shoulder : shoulder region in DTG

T : top side of BIC

t : time

tar : tars

v : volatile matter

w : moisture content

0 : initial condition

∞ : final stage

wb : wet BIC

db : dry BIC

vci : index of pseudo-component in volatile matter

Abbreviations

BIC : bio-coke

mc : moisture content

vc : volatile content

wb : wet BIC

db : dry BIC

TG : thermogravimetry

DTG : derivative thermogravimetry

List of Figures

Chapter 1

Chapter 2

Chapter 3

Chapter 4

Chapter 5

List of Tables

Chapter 1

Chapter 2

Chapter 3

Chapter 1: Introduction

1.1 Overview and significance

Right now, fossil fuels, for example, coal, oil and natural gas represent the prime energy sources in the world, about 80% of the total use of more than 13699 Mtoe (million tons of oil equivalent) [1] per year as shown in Fig. 1.1. But, those fossil fuels are anticipated to be used up during the next few decades. What is more, burning fossil fuel causes environmental harms such as the global warming, acid rain and urban smog due to the production of emissions from fossil fuels, the world has been tempted to try to decrease carbon emissions as much as 80% and turn to find the renewable energy resources (RES) that are more environmentally friendly such as biomass, solar and hydro energy in a sustainable manner [2, 3]. It is reported by Intergovernmental Panel on Climate Change (IPCC) that continued emissions from fossil fuels will result in a temperature increase of between 1.4 and 5.8K over the period from 1990 to 2100 [2].

Within all the renewable energy resources, Biomass has been used for energy resources by the human for a long history. Biomass is a term for all organic material that stems from plants [4], for instance, cropper, weed, wood from forests, residual remained after agricultural and forestry processes, human and animal wastes and so on. From the chemical point of view, it is a composite material, constituted by a mixture of hemicellulose, cellulose, lignin and extractives [4–8]. Due to different chemical structure, biomass is quite diverse. Biomass also includes certain inorganic matter, with a content ranging from less than 1% in wood to 15% in herbaceous biomass and feedstock [9] and up to 25% in some agricultural residues [10]. Ash in the biomass mainly consists of phosphorus, potassium, sodium, silicon, calcium, and

magnesium [11–14]. For some cases, the concentration of chlorine is non-negligible such as herbaceous biomass [13, 14].

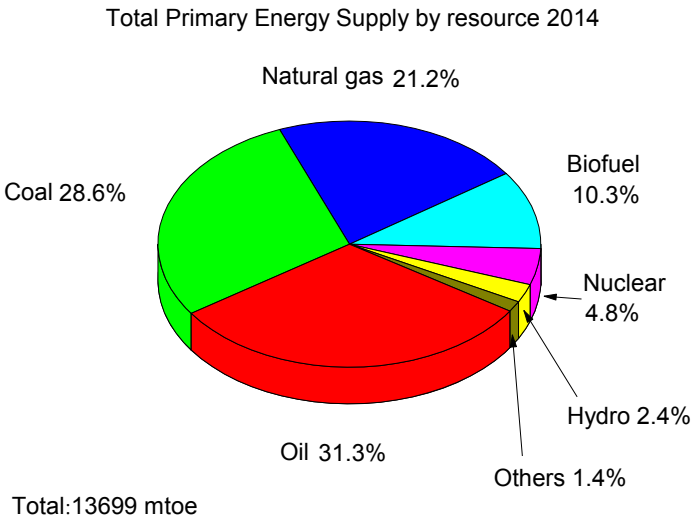

Fig.1. 1 Total primary energy supply by resource in 2014 [1]

In contrast with some other renewable technologies, for instance, solar or hydro energy, biomass has no trouble with energy storage; in another word, biomass is stored energy. The sun's energy when intercepted by plants and converted by the process of photosynthesis into chemical energy, is 'fixed' or stored in the form of terrestrial and aquatic vegetation [15], as shown in Fig.1.2. Moreover, biomass can be treated as versatile fuel, because it can produce biogas, as well as liquid fuels [15]. Due to the unlimited supply, Biomass is a renewable energy source. Crops can be planted continually and waste will always exist. The major advantages of biomass or biomass fuel are shown as below:

(1) Renewable energy source [16]

(2) CO_2 neutral and environment benefits

(3) Usually low contents of N, S and large content of volatile matter [17]

(4) Rich in feedstock

(5) Diversification of fuel supply and energy security

(6) Creation of opportunities and jobs

(7) Co-firing with other fossil fuels [18]

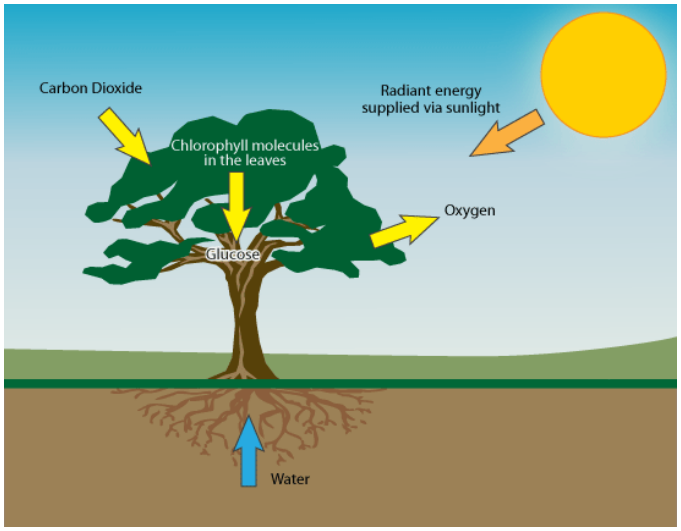

Water + Carbon dioxide + Sun ⟶ Glucose + oxygen

Fig.1. 2 Source of energy in biomass

Based on those merits, biomass fuels become increasingly attractive primary energy source in the world. Biomass contributes 6–14% of the total energy supplies in the developed countries, in contrast, biomass accounts as high as 25% to 34% in developing countries [19]. Biomass is treated as the main energy source in several developing countries, especially in rural regions where biomass is usually the only affordable and accessible energy source and most of it is non-commercial [20]. For example, almost all countries in Southeast Asia are major biomass fuel, especially wood, producers and consumers. Nowadays, wood and other

biomass fuels contribute about 39% of the total energy consumption in the developing countries of the region, and the consumption is still increasing [21].

As for developed country, for example, US, around 3% of all energy consumed in the US consists of biomass sources. In 2002, about 47% of all renewable energy consumed in the US was supplied by biomass. Biomass supplied almost six times the energy of geothermal, solar and wind energy combined [15]. Table 1.1 shows the importance of biomass in the different region.

Table 1. 1 Share of biomass in different regions of the world [15]

Region	Share of biomass in final energy consumption (%)
Africa	60.0
South Asia	56.3
East Asia	25.1
China	23.5
Latin America	18.2
Europe	3.5
North America	2.7
Middle East	0.3

Although biomass is widely accepted in the world, however, issues exist if we utilize directly raw biomass as fuels, for instance, calorific value per unit volume of biomass is low, special treatment is needed to make it less cost for transport and storage. Moreover, controlling the burning rate during combustion is challenging since raw biomass fuel may be inhomogeneous. To overcome these disadvantages, a novel biomass-type fuel has been developed: ‘‘Bio-coke (BIC)” [22–25]. BIC, investigated in the present study, is a highly densified biomass briquette, manufactured by high compression at moderate temperature.

BIC has high mechanical strength and has been shown to be a potential alternative to coal coke. BIC can be manufactured in a wide range of sizes, including large dimensions, and with densities higher (1300 kg/m^3) than those with ordinary wood pellets (600 kg/m^3) [26]. This slows the combustion of the fuel, thus enabling a longer heat release period and resulting in a better overall performance than that obtained with existing biomass fuels. Because of its high volumetric calorific value and mechanical strength, BIC also has relatively low transport and storage costs, the detailed information about BIC will be shown in Chapter 2.

1.2 Summary of previous works

Since BIC is newly developed fuel, besides our group, there is little research about the combustion behavior of such highly densified biomass briquette. However, many researchers studied the combustion characteristics (including drying and pyrolysis process) of different sorts of biomass fuel. In this Section, firstly, we will introduce our previous study about BIC. Then, the detailed mechanism of pyrolysis of biomass or wood is explained. Finally, the combustion characteristics of different sorts of biomass fuel are shown and discussed.

1.2.1Previous studies of BIC

At the beginning, Hiroyuki Ito et al. [25] investigated the ignition behavior of Bio-coke (BIC) in high-temperature air flows (473-873 K, 9.17-12.50 NL/s.) experimentally. In the experiments, preheated air was blown onto the bottom surface of BIC cylinders and the ignition behavior of the bottom surface was observed monitoring the surface temperature as well as the time-dependent mass loss rates. The results show two ignition modes; (1) solid surface ignition preceding gas-phase ignition in high air temperature conditions (T≥598K),

and (2) gas-phase ignition accompanied by simultaneous surface ignition occurring at relatively low air temperature conditions. The appearance of each mode depends on the preheated air supply condition in terms of the air temperature, flow velocity, and moisture content of the fuel. The rate of evolution of volatile gasses is closely correlated with the temperature distribution inside the BIC briquette which depends on the heating rate, implying that variations in the temperature distribution inside the fuel could be one reason for the appearance of the observed ignition modes. It is suggested that the temperature distribution inside the fuel has to be taken into account in the control of the ignition behavior of BIC briquettes.

Then, Nakahara et al. [27] designed an end-face combustion setup for BIC and conducted several experiments to study one-dimensional steady combustion of Bio-coke in air flow. In the experiments, the air flow velocity was the main test condition and the fuel consumption rate when the bottom surface of the BIC sample burned was evaluated as the regression rate of the combustion zone at the bottom surface. The results showed that steady combustion of the BIC sample could be attained in 4.67 m/s or more, and, in contrast, extinction was observed in 3.82 m/s or less. The critical regression rate explained by the combustion zone temperature was shown, and the reason combustion becomes unsteady could be explained by the energy balance at the combustion zone. The main reason for extinction was radiation heat loss.

1.2.2 Pyrolysis of biomass or wood

Pyrolysis, as one of the most important processes during solid combustion, consisting of solid thermal degradation in the absence of oxidizing agents, is a possible thermochemical conversion route, leading to the produce huge chemical compounds. Nevertheless, for

applications, we often lump the reaction products into three groups: tar, permanent gases and char [28], or just simply into volatile gases and char.

There are several ways to get the global or semi-global mechanisms of Pyrolysis of biomass or wood, among them, thermogravimetric analysis is one the most popular way. According to thermogravimetry experiment (slow heating rates for a sufficiently small mass of the sample, so that a kinetic control is established), the main degradation of biomass usually starts at about 500 K, and the process is practically terminated at 700–750K [29–31]. The mass loss stems from the activity of several reactions. Hence, thermogravimetric curves, obtained from dynamic or isothermal conditions, are of great importance for obtaining the global or semi-global mechanisms.

1.2.2.1 One-component mechanisms of primary pyrolysis

As already discussed, weight loss curves of biomass, gained under dynamic or isothermal conditions, show different reaction regions mainly corresponding to component degradation, the kinetic mechanisms include a single or three parallel reactions for the formation of the main product classes (one-stage or one-component mechanisms) following the proposal by Shafizadeh and Chin [32] for wood (Fig. 1.3).

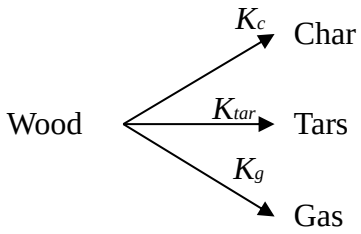

$K = K_c + K_{tar} + K_g$

Fig.1. 3 One-component mechanisms of primary wood pyrolysis

It presents a summary of the one-component mechanisms of biomass or wood pyrolysis

based on experiments carried out under different conditions in Table 1.2. It appears that the values of activation energy (E) of the global reaction are widely scattered, roughly between 50 and 175 kJ/mol, which could be explained as the result of the different heating conditions in experimental devices, such as tube furnaces, screen heaters, classical thermogravimetry and so on, the different sample property (size, feedstock and so on) and the mathematical method of the experiment data.

Table 1. 2 Kinetic parameters for one-component mechanisms of wood or biomass pyrolysis

Author	Feedstock	Experiment system	Temperature	Kinetic constant
Thurner et al.[33]	Oak, 650 μm	Isothermal tube furnace	573–673K	$K_c=7.4\times10^5 exp(-106.5/RT)$ $K_{tar}=4.12\times10^6 exp(-112.7/RT)$ $K_g=1.43\times10^4 exp(-88.6/RT)$
Gorton et al.[34]	Hardwood,300–350 μm	Isothermal entrained-flow reactor	677–822K	$K=1.483\times10^3 exp(-89.52/RT)$
Wagenaar et al.[35]	Pine,100–125 μm	Drop tube	773–873K	$K_c=3.05\times10^7 exp(-125/RT)$ $K_{tar}=9.28\times10^9 exp(-149/RT)$ $K_g=1.11\times10^{11} exp(-177/RT)$
Ward et al. [36]	Wild cherry	Isothermal tube furnace	538–593K	$K=11.9\times10^{11} exp(-173.7/RT)$

1.2.2.2 Multi-component devolatilization mechanisms

Multi-component mechanisms usually contain parallel reactions (Fig. 1.4) for the degradation of the pseudo-components, for a single pseudo-component, whose mass fraction is one of model parameters, it has no interactions with other pseudo-components. Among all the multi-component mechanisms, three-component devolatilization mechanism is the most popular one, which includes hemicellulose, cellulose and lignin.

$$Y_{vci} \longrightarrow g_{vci} \qquad k_{vci} = A_{vci}\, exp(-E_{vci}/RT) \qquad vci = 1,n$$

Fig.1. 4 Multi-component devolatilization mechanisms (Y_{vci} is the volatile fraction of the *vci*th pseudo-component)

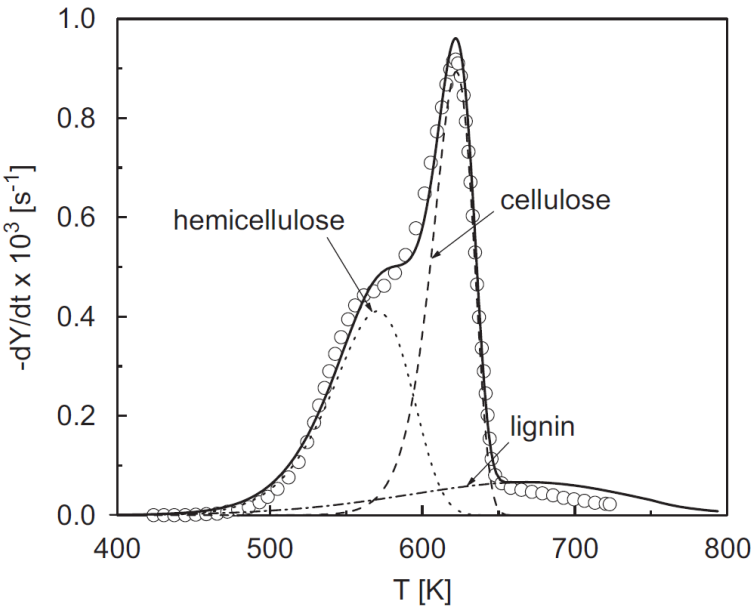

Fig.1. 5 Comparison between the experimental (symbols) and calculated DTG curves (solid line) for beech wood heated at 5 K/min, by means of a three-component devolatilization model. [41]

The three-component mechanism with linear or nonlinear dependence on species concentrations, for the volatile fractions of the pseudo-components hemicellulose, cellulose and lignin, is widely applied [29,37–40] to describe dynamic thermogravimetric curves of wood or biomass devolatilization. In many cases, only one heating rate is examined by dynamic mass loss measurements and the corresponding kinetic analyses, usually less than 10 K/min [37, 40, 41]. It shows that the by the process simulations that there is no interacting between the decomposition of pseudo-components hemicellulose and cellulose, the shoulder of the rate curves is associated with hemicellulose and cellulose contributes mainly to the peak of the curves, the lignin, in contrast, has a slow decomposition rate over a wide temperature range. It shows one example in Fig. 1.5, under a heating rate of 5 K/min for

beech wood [41]. It shows good agreement of the differential curves by experiment and derived kinetic parameters. According to the reference[41], the activation energies of hemicellulose change between 80 and 116 kJ/mol, 195–286 kJ/mol for cellulose, and 18–65 kJ/mol for lignin. Meanwhile, the mass fraction of each component is shown as hemicellulose roughly accounts for 20–30% of the total mass, cellulose is around 28–38% and lignin occupies about 10–15%.

1.2.3 Combustion of biomass or wood

There are numerous researches about the combustion behavior of biomass or wood, we briefly introduce some of them in the following part.

Ali Rostami et al. [42] investigated the smoldering process numerically in a porous biomass fuel rod, a transient axisymmetric two-dimensional (2D) model was developed for the forward and natural smoldering of a porous biomass fuel rod. The model includes two parts: kinetic modeling of pyrolysis and combustion reactions and CFD modeling of the flow and energy equations. Heat transfer is represented by two energy equations whereby the solid and gas phases are considered to have separate and distinct temperatures interacting through an interface heat exchange. The starting material first undergoes pyrolysis prior to oxidation of the remaining carbonaceous residue. The pyrolysis is assumed to consist of a set of first-order reactions. Oxidation of the carbonaceous residue is accompanied by the formation of gas-phase combustion products, the concentration of which is also computed. Calculations under unsteady conditions are done for both natural and forward smoldering for a variety of operating and boundary conditions as well as physical properties of the fuel and the packing density. The computation captures the development of a steady combustion region in which it moves at a constant rate. The results for the gas and solid temperature profiles, oxygen

concentration profile and pressure distribution are also presented. The effects of surface heat loss, heating value of fuel, airflow rate, porosity of the fuel rod on temperature and smolder velocity are discussed.

Ouedraogo et al. [43] established a shrinking core model of the combustion of individual chunk wood and particle wood elements, the model is formulated on the physical evidence that large wood specimens inserted into a hot convective environment lose weight mostly over a relatively thin outside layer, while the interior (core) remains relatively undisturbed. The modeling of the complete process requires a correlation of the turbulent heat and mass transfer coefficients which include explicitly the effects of transpiration of volatilized organic compounds and moisture, along with geometry, and equivalent radius. The fuel element burnout time is shown to be a function of fuel properties, moisture content, and size. Drier and smaller elements burn faster. Moisture is shown to slow the shrinking rate due to the cooling effects of transpiration and the latent heat of evaporation.

Yang et al. [44] investigated effect of air flow rate and fuel moisture on the burning behaviors of biomass and simulated municipal solid wastes in packed beds, in their research, mathematical simulations as well as experiments have been carried out for the combustion of wood chips and the incineration of simulated municipal solid wastes in a bench-top stationary bed and the effects of primary air flow rate and moisture level in the fuel have been assessed over wide ranges. It is found that volatile release as well as char burning intensifies with an increase in the primary air flow until a critical point is reached where a further increase in the primary air results in slowing down of the combustion process; a higher primary airflow also reduces the char fraction burned in the final char-burning-only stage, shifts combustion in the bed to a more fuel-lean environment and reduces CO emission at the bed top; an increase in the moisture level in the fuel produces a higher flame front temperature in the bed at low

primary air flow rates.

Again, their group investigated fuel size effect on pinewood combustion in a packed bed [45]. In this study, particle size effect on pinewood combustion in a stationary packed bed was investigated. Mass loss rate, temperature profile at different bed locations and gas compositions in the out-of-bed flue gases were measured at a fixed primary air flow rate. Pinewood cubes was fired with size ranging from 5 to 35 mm. A unique numerical model applicable to thermally thick particles was proposed and relevant equations were solved to simulate the non-homogeneous characteristics of the burning process. It is found that at the operating conditions of the current study, smaller particles are quicker to ignite than larger particles and have distinctive combustion stages; burning rate is also higher with smaller fuel size; and smaller fuels have a thinner reaction zone and result in both higher CO and CH_4 concentrations in the out of bed flue gases; on the other hand, larger particles produced a higher flame temperature and result in higher H_2 concentration in the flue gases. Larger particles also cause the combustion process becoming more transient where the burning rate varies for most part of the combustion process.

Demirbas[46] made a summary of combustion characteristics of different biomass fuels, he explained the gasification and pyrolysis reaction of different biomass, he also paid attention to the combustion properties of biomass and cofiring of biomass and coal blends.

There are a huge number of researches about biomass and wood, however, BIC is a newly developed fuel with quite a unique characteristic such as large density, which has not been studied extensively before, so it is worth to study the combustion behavior of BIC in detail.

1.3 Objective of present research

In this section, we explain the motivation of this research. Briefly, we aim to get the better knowledge of the combustion behavior of BIC and achieve better controlling of combustion behavior of BIC. Driven by the motivation, what kind of specific work relative to this research is discussed.

1.3.1 Motivation

As shown in section1.1, besides owning the same merit as other biomass fuel, BIC possesses some unique characteristic, including large density, high volumetric calorific value, high mechanical strength and so on. Because of its outstanding characteristics, BIC has been introduced into many sectors as a heating source, including iron smelting and agricultural greenhouses. However, new challenges have arisen. The constant temperatures that must be maintained inside greenhouses in cold regions require a constant heat release rate from the furnace when using BIC as the fuel. To satisfy this requirement, the authors have proposed the end-face combustion of BIC [27], wherein one end face of the BIC is burned one-dimensionally. This combustion method makes steady heat release possible, thus allowing a constant temperature to be maintained in the greenhouse over a long period. Our previous study [27] showed that under a certain condition, steady combustion can be obtained. However, under some other conditions, before steady combustion is reached, the fuel goes through a transient combustion period, and in this phase, the regression rate is not stable. Considering the importance of steady combustion, this transient combustion is also another important research topic, which has not been extensively investigated in previous studies. Galgano and Blasi [47] established a one-dimensional shrinking unreacted core model for

investigating the propagation of drying and decomposition fronts in wood exposed to thermal radiation. They showed that, in the case of thick samples, the drying and conversion times have an almost linear dependence on initial moisture content. However, they only investigated the evolution of the temperature distribution inside the wood and did not consider the combustion process of char, although the system they investigated was similar to ours. Few other studies are available on the end face combustion of solid biomass fuel and the effect of unsteady combustion. It also allows us to gain a better understanding of the combustion characteristics of this novel biomass fuel and the design of a combustion furnace.

1.3.2 Scope of present research

In the present study, based on end-face combustion method, the combustion behavior of BIC, including the steady and transient combustion were discussed under different conditions, for instance air flow rate, air temperature, volatile content and moisture content of BIC, the density of BIC. We try to figure out the mechanism controlling transient combustion and reveal whether steady combustion can be obtained or not.

The brief introduction of each of the following chapters in this thesis is shown as follows:

In Chapter 2, we introduced the properties of BIC, including the feedstock of BIC, density, composition of BIC.

In Chapter 3, the end-face combustion experimental setup was shown also well as the one-dimensional numerical model. The kinetic parameters of drying and pyrolysis reaction of BIC were obtained.

In Chapter 4, steady combustion of BIC was discussed both in calculation and experiment, the extinction limits was shown under different conditions in steady combustion.

In Chapter 5, end-face combustion in the transient period between ignition and steady combustion has been investigated. A one-dimensional numerical model was established to study the change of regression rate and temperature distribution in BIC samples placed in opposed convective air flow and compared with experimental findings. Moreover, the mechanism for controlling the transient characteristics of BIC end face combustion and the role of the various parameters in the transient combustion stage was investigated.

Chapter 6 is the summary.

Chapter 2: Properties of Bio-coke (BIC)

In Chapter 2, we presented the important information of BIC including feedstock, manufacture process, density, elemental analysis, proximate analysis of BIC.

2.1 Feedstock and manufacture procedures of BIC

Japanese knotweed (Fig.2.1) was selected as the feedstock for BIC in this study as it is rich in Japan and almost free of charge. The detailed procedures for making BIC [49] are reported in Table 2.1, briefly, harvested Japanese knotweed was pulverized, stuffed into cylindrical molds, pressed and heated simultaneously, and subsequently cooled to room temperature. After cooling, the cylindrical solid BIC briquette was removed from the mold. Since cellulose, hemicellulose and lignin are the main structure composition of biomass, and the lignin improves the binding property of the biomass briquettes during densification and heating process, because the melting point of lignin is quite low. When heating up the biomass, lignin becomes soft and melts, which leads to thermosetting [50]. Meanwhile, the self-bonding property is again enhanced by the furfural derived from hemicellulose [51]. The BIC briquette, resulting from the densification under certain pressures and temperatures, is a large block of biomass possessing high mechanical strength and large density.

Fig.2. 1 Japanese knotweed [48]

The dimensions of the BIC (Fig.2.3) used in the present study are 0.048 m in diameter and 0.085 m in length. An outstanding property regarding combustion characteristics is its high density (1300 kg/m^3, for wood pellets 600 kg/m^3 [26]).

Table 2. 1 Manufacture procedures of BIC

● Drying and pulverizing	Harvested Japanese knotweed is air-dried and pulverized to powder with the diameter of several mm.
● Padding	The pulverized knotweed (0.2kg) is stuffed into cylindrical molds (Fig.2.2).
● Heating and compression	The pulverized knotweed is electrically heated up to 423K, and maintain the temperature for 15 minutes, with 22Mpa pressure in the axial direction.
● Cooling	Stop the heater, natural cooling with 22Mpa pressure in the axial direction.
● Remove	Stop compression, BIC is removed from the cylindrical molds.

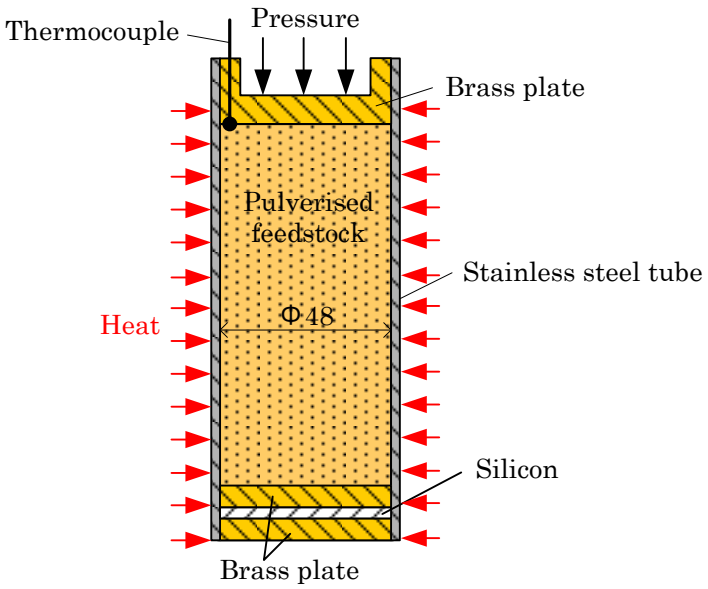

Fig.2. 2 Cylindrical molds

Upper side	Side	Bottom side
		

Fig.2. 3 Bio-coke sample in present research

2.2 Elemental analysis

Elemental analysis helps to obtain the mass fraction of N, S and Cl to assess the environmental impact of the fuel. Furthermore, it helps to detect the percentage of carbon, hydrogen and oxygen to calculate the heating value of the fuel.

Figure 2.4 shows the process of elemental analysis for BIC, the detailed elemental analysis process can be found on the web [52].

Table 2.2 shows the results of elemental analysis of different types of solid fuel, as can be seen, the main elements consisting BIC are C, H, O (if we allocate that all the remain part to O), C accounts for 47.72% of total weight, H is 5.95%, N is 0.47%, while the contents of S and Cl are almost negligible, which are lower than the detection limit (0.3wt%), the content of O is about 38.08% (difference value).

Base on those data, we can obtain the calorific value of BIC (HHV): 17.9 MJ/kg, Compare with fossil fuel, BIC has lower calorific value, this is due to less content of C inside BIC, as shown in Table 2.2, the content of C is 47.72% for BIC while 77.22% for bituminous coal and 50.3% for wood pellets.

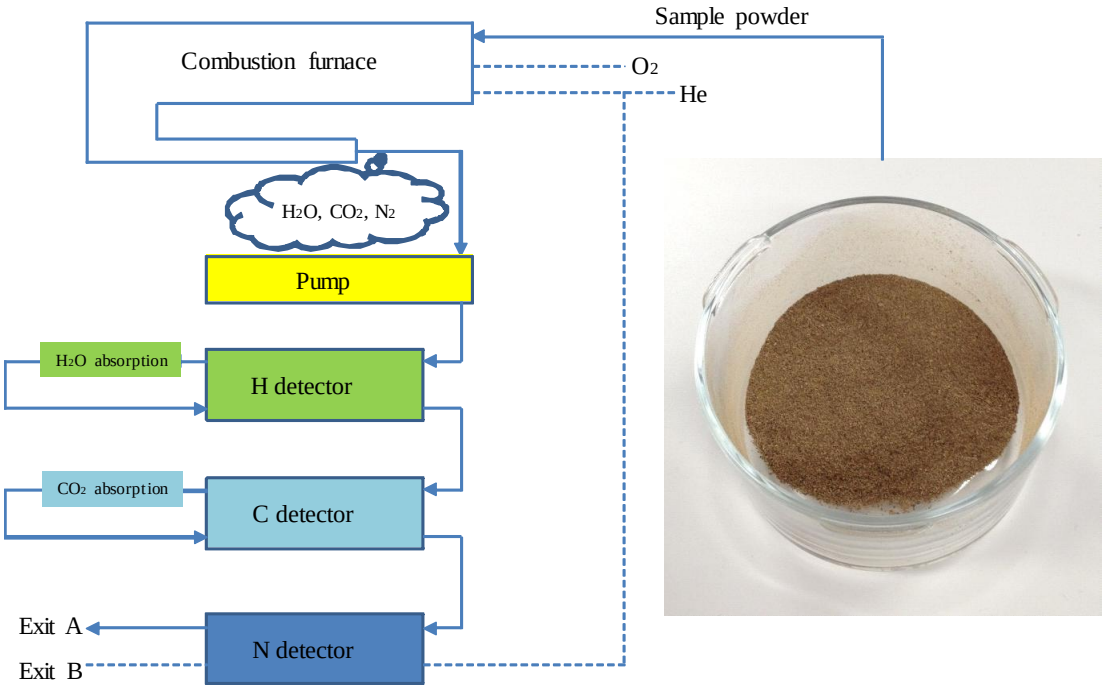

Fig.2. 4 Elemental analysis process [52]

Table 2. 2 Elemental analysis of different solid fuel (Dry basis)

	Japanese knotweed	Wood pellets[26]	Bituminous coal[53]
C [wt%]	47.72	50.3	77.22
H [wt%]	5.95	5.7	5.6
N [wt%]	0.47	0.22	1.31
S [wt%]	< DL	-	-
Cl [wt%]	< DL	-	-

DL: detection limit, 0.3wt%.

2.3 Proximate analysis

Proximate analysis helps to obtain the mass fraction of moisture, volatile matter, fixed carbon and ash contents. This analysis is of great importance to investigate the combustion phenomenon of solid fuel. For instance, high ash contents in solid fuel may lead to ignition problems as well as slagging problems, which is due to the low melting point of the dissolved

ash. The high volatile content of the biomass provides a number of advantages as combustion resource. What is more, high fixed carbon content and volatile matter enhance the heating value of biomass fuel.

In our proximate analysis, thermogravimetric experiments [25] were carried out to obtain the thermo-chemical characteristics of the BIC. 20 mg specimens of the pulverized BIC extracted from the bottom center (bottom surface) of the BIC, which is to be exposed to the preheated air in the combustion experiments described later, were heated by a radiant heater with a heating rate of 5K/min and the mass loss of the specimen was measured in an ULVAC TGD-5000 thermo-balance. Figure 2.5 shows the results of the thermogravimetric analysis both in air and nitrogen atmosphere. From the results the water content could be estimated to be about 10.0 wt% due to the mass loss observed below 400 K. The content of fixed carbon can be estimated at about 13.0 wt% from the difference between the mass losses in N_2 and air at around 900 K. The content of ash is approximated about 7.0 wt%, and therefore, the content of volatile matter can be estimated as 70.0 wt%.

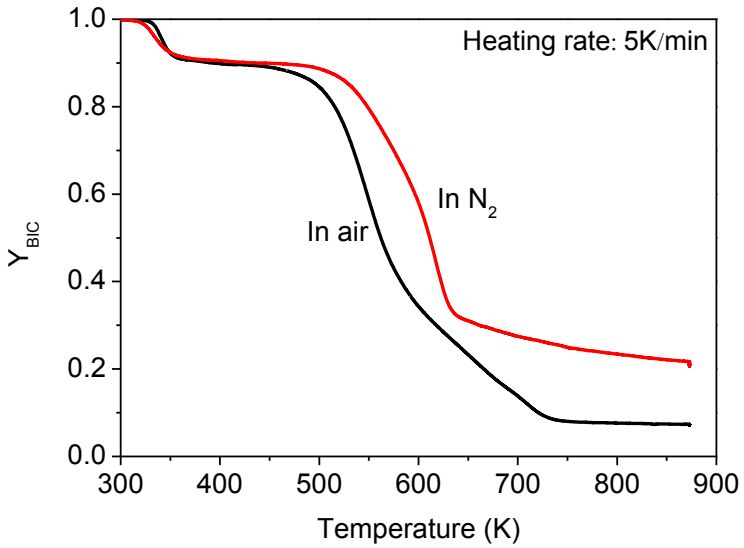

Fig.2. 5 TG analysis of BIC [25]

From the comparison between the curves for air and nitrogen, it is found that differences caused by oxidation appear when the temperature exceeds around 450K, which indicates the oxidative pyrolysis takes place when temperature is higher than 450K.

Table 2.3 shows proximate analysis of different types of biomass, as can be seen, moisture content of BIC is 10.0%, a little higher than moisture content in wood (6.2%) and wheat straw (6.6%). Volatile content accounts for 70.0% of BIC total mass, however, for wood and wheat straw, volatile contents are 68.9% and 66.4%, respectively. As for the fixed carbon, 13.0% of total mass of BIC is fixed carbon, which is lower than that in wood (24.2%) and wheat straw (17.7%).

Table 2. 3 Proximate analysis of different solid fuel (Air dry basis)

	Japanese knotweed	Wood[54]	Wheat straw [55]
Moisture [wt%]	10.0	6.2	6.6
Volatile content [wt%]	70.0	68.9	66.4
Fixed carbon [wt%]	13.0	24.2	17.7
Ash [wt%]	7.0	0.7	9.3

2.5 Concluding remarks

In this Chapter, we presented the properties of BIC including feedstock, manufacture process, density, elemental analysis, proximate analysis of BIC.

The dimensions of BIC used in present study are 0.048m in diameter and 0.085m in length, density of BIC is 1300kg/m^3.

According to elemental analysis, the main elements of BIC are C (47.72%), H (5.95%),

N (0.47%) and Cl and S belong to a negligible level, the heating value of BIC is 17.8MJ/kg.

According to proximate analysis, moisture accounts for 10.0% of total mass, volatile content accounts for 70.0%, fix carbon is 13.0% and ash is 7.0%.

Chapter 3: Experimental setup and numerical model

In this Chapter, we introduced the end-face combustion experiment setup which makes quasi-one-dimensional combustion behavior of BIC possible. Then one-dimensional calculation model based on the end-face combustion experiment setup was presented. Finally based on the thermogravimetric curves, we obtained the kinetic parameters of drying reaction and pyrolysis reaction by means of multi-component devolatilization mechanisms and one-component mechanisms of primary pyrolysis, respectively.

3.1 Experimental setup

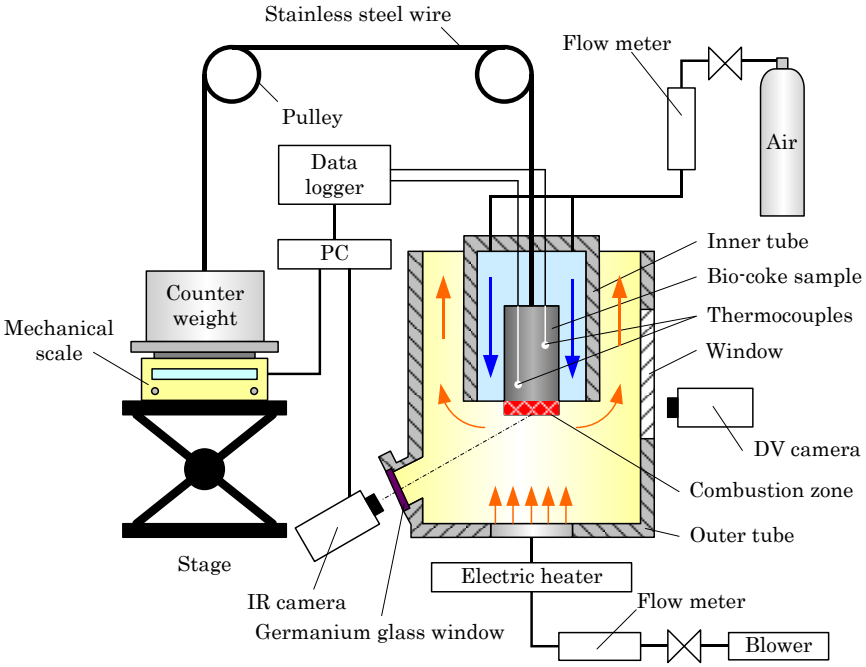

Fig.3. 1 Schematic drawing of the experimental setup

The experimental apparatus is schematically outlined in Fig. 3.1. It consists of (a) a combustion chamber, (b) an air supply system, (c) a cooling system which protects the side

wall of BIC sample from heating up, (d) a scale for measuring the mass loss of the BIC, (e) an infrared camera which records the bottom surface temperature of the BIC, (f) a digital video camera which monitors the combustion behavior of the BIC, and (g) thermocouples to measure the temperature inside BIC sample. The combustion chamber (Fig. 3.2) includes an inner chamber and an outer chamber, the outer chamber is a tube made of stainless steel with the diameter of 0.1m, the diameter of the inner combustion chamber where BIC is located is 0.049m, the inner combustion chamber contains a pathway for air cooling system. A stainless steel bar (0.008 m outer diameter) is screwed into the top of the BIC and this is suspended from an arm of the fulcrum. The BIC sample is located at the center of the inner combustion chamber. Air is metered and subsequently heated by the electric heater and blown onto the bottom surface of the BIC. An R-type thermocouple (0.0003 m diameter) is employed to measure the gas temperatures near the top and bottom edges of the BIC. The junctions are located about 0.001 m from the respective edges. The air supply temperature is determined by monitoring the temperature at the exit of the electric heater. The mass loss of the sample is monitored by a mechanical scale (SHIMADZU, UX4200H: minimum scale value 0.01g). Five thermocouples are placed around the circumference of the 0.024-m-diameter circle and at every 0.01 m in an axial direction from the initial location of the bottom surface (Fig. 3.3).

Temperature changes at the bottom surface of the BIC are observed by the infrared camera (NEC Sanei, TH6200R, 8-14E-06 m, below 1273K) through a Zn-Se glass window. The maximum temperature of the BIC bottom surface is termed the "BIC bottom surface temperature". The ignition and combustion behavior are recorded by the digital video camera (SONY DCR- TRV900) through quartz glass windows. The air temperature and air flow rate are varied within the range of 573-873 K and 5.83-12.50 NL/s (350-750NL/min), respectively.

Above is the end-face combustion setup, due to the special design, quasi-one-

dimensional combustion behavior of BIC inside the combustion chamber is possible (Fig. 3.4), the combustion behavior of BIC will be a one-dimensional regression.

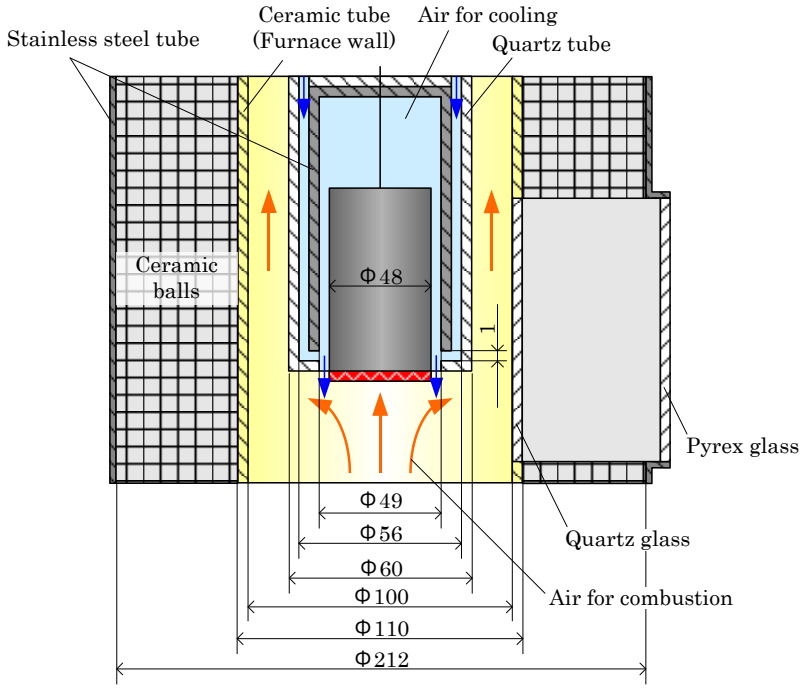

Fig.3. 2 Schematic drawing of the combustion chamber

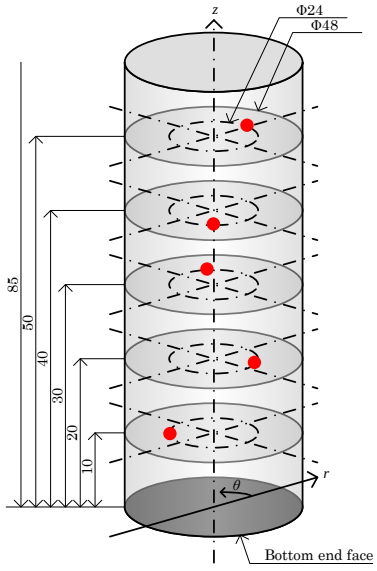

r [m]	θ [deg.]	z [m]
0.012	144	0.010
0.012	288	0.020
0.012	72	0.030
0.012	216	0.040
0.012	0	0.050

●: Measuring points

Fig.3. 3 Locations of five thermocouples inside BIC sample

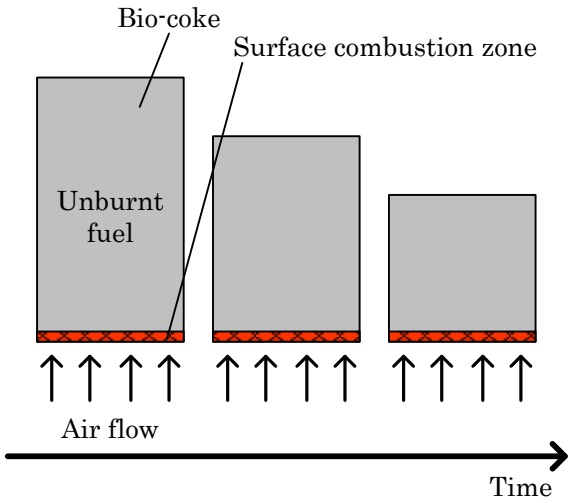

Fig.3. 4 End-face combustion of BIC

3.2 Numerical model

3.2.1 Governing equations

In the present study, a BIC sample was treated as a one-dimensional model with four condensed phases (wet BIC, dry BIC, char, and ash) considering the transport of decomposition gas inside the BIC. The origin of the calculation coordinate was at the bottom (Fig. 3.5). The gas phase outside the decomposing sample was not included in the model. The assumptions were as follows:

- Every condensed phase has well-defined properties: specific heat capacity and thermal conductivity.
- In the conservation equations, the thermal dynamic properties can be calculated by appropriate mass weightings, $c_{p,s} = \sum Y_j c_{p,j}$ and $\lambda_s = \sum Y_j \lambda_j$.
- A local thermal equilibrium exists between the gas and condensed phases.
- Once the decomposition gas is formed, it is transported through the char layer to the bottom surface and then released.

- The char oxidative reaction is treated as a surface reaction.

The conservation equations resulting from these assumptions are given as Eqs. (3-2) and (3-3):

Condensed phase mass conservation:

$$\frac{\partial \rho_s}{\partial t} = -(\omega_w + \omega_v + \omega_c/\Delta x) \quad (3\text{-}2)$$

Condensed phase energy conservation:

$$\rho_s c_s \frac{\partial T}{\partial t} = \lambda_s \frac{\partial^2 T}{\partial x^2} + Q_w \omega_w + Q_v \omega_v + Q_{sg} \quad (3\text{-}3)$$

In Eq. (3-2), Δx is the length of grid, and in Eq. (3-3), Q_{sg} is the heat transfer between the solid and gas phases inside the BIC, as defined in Eq. (3-4)

$$Q_{sg} = \dot{m}'' c_{p,g} \frac{\partial T}{\partial x} \quad (3\text{-}4)$$

Here, $c_{p,g}$ is the specific heat of decomposed gas inside the BIC. For grid g*i*, $\dot{m}''$ (see Fig. 3.5) is the mass flux of decomposition gas transport from grid g*i* + 1 to grid *i*, $\dot{m}''_{gi} = \dot{m}''_{gi+1} + (\omega_v(gi+1) + \omega_w(gi+1))\Delta x$.

3.2.2 Initial and boundary conditions

Initial condition:

$$T(gi) = 300;\ \rho_j(gi) = \rho_{j,0} \quad (3\text{-}5)$$

Top boundary condition:

$$\left.\frac{\partial T}{\partial t}\right|_T = 0 \quad (3\text{-}6)$$

Bottom (combustion side) boundary condition:

$$H(T_{air} - T_B) = \lambda_s \left.\frac{\partial T}{\partial x}\right|_B - Q_c \omega_c + \varepsilon\sigma(T_B^4 - T_{am}^4) + \dot{m}''_B h \quad (3\text{-}7)$$

In Eq. (3-7), $\dot{m}''_B$ is the decomposed gas flux released from the bottom surface, given as $\dot{m}''_B = \dot{m}''_1 + (\omega_v(1) + \omega_w(1))\Delta x$. H is the heat transfer coefficient. A blowing effect

occurred at the bottom side boundary, wherein the decomposed gas flux blowing from the bottom surface made it more difficult for oxygen to penetrate the sample surface [59]. As shown in Eq. (3-8), the effect of blowing on the heat transfer coefficient *H* was estimated with the Couette approximation [60]:

$$H = \frac{\dot{m}_B'' c_{p,g}}{\exp(\dot{m}_B'' c_{p,g}/H_n)-1} \quad (3\text{-}8)$$

Here, H_n is the bottom surface heat transfer coefficient without blowing.

3.2.3 Kinetic model

Three condensed phase reactions were modeled, derived by Eq. (3-9)–(3-11). The drying process of the BIC is modeled in Eq. (3-9). In Eq. (3-10), the dry BIC is converted to char, and in Eq. (3-11), the char converts to ash, thus consuming oxygen in the process and producing carbon dioxide and carbon monoxide.

[Wet BIC] → φ_{db} [Dry BIC] + φ_w [Water Vapor] (3-9)

[Dry BIC] → φ_c [Char] + φ_v [Pyrolysis Gas] (3-10)

[Char] + φ_{o_2} [O_2] → (1 + φ_{o_2}) [Char Oxidation Products] (3-11)

The drying and pyrolysis reaction rates are expressed in Eqs. (3-12) and (3-13), respectively.

$$\omega_w = \rho_w A_w \exp(-E_w/RT) \quad (3\text{-}12)$$

$$\omega_v = \rho_v A_v \exp(-E_v/RT) \quad (3\text{-}13)$$

The char oxidation reaction is treated as $c + \varphi_{o_2} o_2 = 2(1 - \varphi_{o_2})co_2 + (2\varphi_{o_2} - 1)co$. The ratio of co to co_2 varies with temperature at $\tau = 2500\exp(6420/T)$, as proposed by Evans and Emmons [61]. The reaction rate is expressed in Eq. (3-14):

$$\omega_c = \frac{C_{o_2,am}}{(1/K+(\theta\times\varphi_{o_2})/H_d)} \quad (3\text{-}14)$$

K is the char oxidative reaction kinetic constant, and H_d is the mass transfer coefficient. $K = A_c \exp(-E_c/RT)$, and $H_d = H/c_{p,g}$. θ is defined as the molecular weight ratio between oxygen and char, where $\theta = M_{o_2}/M_c$.

The char combustion heat [62] depends on τ, which represents the ratio of co to co_2.

$$Q_c = 3.3 \times 10^7 \times \frac{1}{1+\tau} + 1.1 \times 10^7 \times \frac{\tau}{1+\tau} \quad (3\text{-}15)$$

The char oxidative reaction kinetic parameters were taken from [63].

3.2.4 Regression condition

The regression condition is defined as follows: apart from the ash, 95% of the other material is consumed in the local grid. The computational cell in the solid is considered to be consumed and is excluded from the calculation.

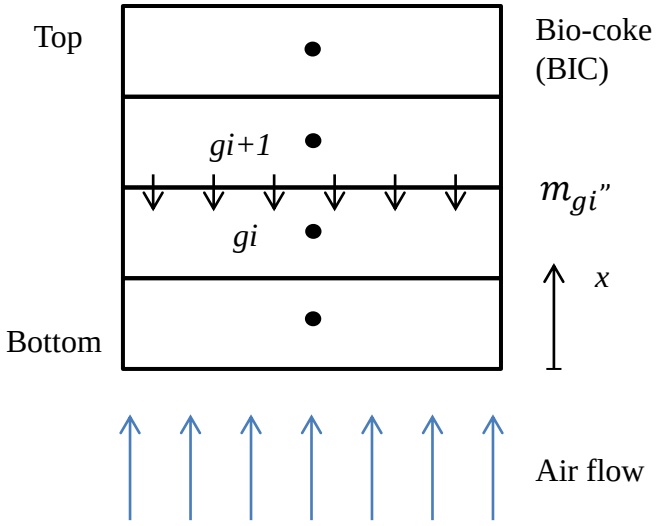

Fig.3. 5 Control volume system used for calculation

3.3 Kinetic parameters of drying and pyrolysis reaction of BIC

Based on the TG data, BIC is one kind of biomass renewable resource contains non-negligible moisture content and high volatile content, in BIC combustion or smoldering, evaporation temperature or decomposition temperature is reached firstly during heated, drying and pyrolysis are main reasons for the mass loss of BIC. Meanwhile, moisture evaporation stage acts as a heat loss term and impedes the decomposition and combustion processes, pyrolysis produces lots of combustible gases, oils, and solid carbon-containing residues which play important role in the combustion [61]. So it is important to study the drying and pyrolysis processes.

3.3.1. Experimental Results.

Figure 3.6 shows the experimental thermogravimetry (TG) and derivative thermogravimetry (DTG) plots for BIC drying and pyrolysis in nitrogen at heating rates of 5 K/min.

The first mass loss phase took place from around 320K to about 400K, contributing around 10% of the total mass loss for the experiment at heating rates of 5 K/min. The peak of mass loss showed around 350 K, and the maximum normalized mass loss rate was 0.0002 s^{-1}, it is speculated that this mass loss phase is due to evaporation of moisture content.

The next mass loss phase happened within the temperature range of about 450-800 K. In this phase, the organic components of BIC decomposed. When temperature increasing from 450K, the decomposition rate of organic component reached the local maximum (0.00065 s^{-1}) at 620 K, following by a rapid decrease in decomposition rate , After 700 K, the sample mass slowly decreased and implied the termination of that the decomposition of organic

components. We need to pay attention to the temperature period from 575K to 600K, it showed a clear shoulder region in DTG curve, which indicates within that temperature period, overlap takes place between different independent reactions. So it is meaningful to investigate the decomposition characteristics of BIC in detail.

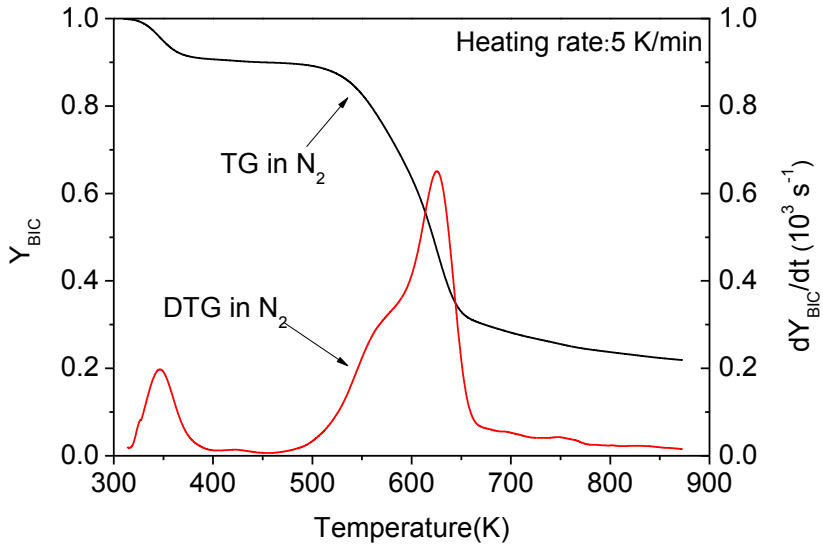

Fig.3. 6 TG and DTG curves of BIC pyrolysis in nitrogen at heating rates of 5 K/min

The decomposition characteristics of BIC can be interpreted by several parameters, which strongly depend on the temperature ranges of the different zones of the weight loss curves. The mass fraction and the first and second time derivatives of the mass fraction are important evidence for such definitions as shown in Fig.3.7. The initiation of hemicellulose decomposition was related to $T_{onset(hc)}$ defined by extrapolating the slope of the devolatilization rate in correspondence with the first local maximum in $-d^2Y/dt^2$ (up to the zero level of the Y axis). Given the appearance of a shoulder, the decomposition temperature of the hemicellulose was characterized by $T_{shoulder}$, defined by the point where $-d^2Y/dt^2$ attained the value nearest to zero in this region. For the cases when the hemicellulose and

cellulose decomposition were less overlapped, the parameter $T_{shoulder}$ marked the peak top of the hemicellulose decomposition. The corresponding devolatization rate, $-(dY/dt)_{shoulder}$, and mass fraction, $Y_{shoulder}$, can be easily evaluated. The temperature T_{peak}, where the maximum devolatilization rate was attained (associated mainly with cellulose decomposition), was also introduced with the corresponding $-(dY/dt)_{peak}$ and Y_{peak}. The maximum of the final, tailing region dominated by the lignin decomposition, was identified by $T_{offset(l)}$, which was obtained by extrapolating the devolatilization rate corresponding to the local minimum in $-d^2Y/dt^2$ in this region (again up to the zero level of the Y axis).

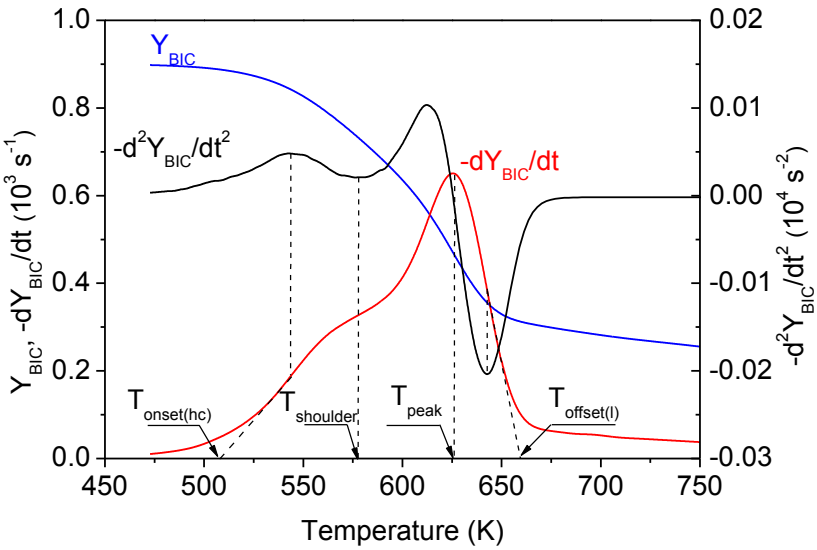

Fig.3. 7 Mass fraction and first and second time derivatives of the mass fraction as functions of temperature for BIC and definitions of the characteristic reaction temperatures

Base on the explanation above, the devolatilization characteristics for BIC is given in Table 3.1. As can be seen, the decomposition of hemicellulose started from 500K ($T_{onset(hc)}$), and reached the maximum devolatilization rate when temperature was 580K ($T_{shoulder}$). As for cellulose, we could only find that the maximum devolatilization rate of cellulose appeared

when temperature reached 625K (T_{peak}). As for lignin, that the maximum devolatilization rate of cellulose could be obtained when temperature reached around 670K ($T_{offset(l)}$).

Table 3. 1 Degradation characteristics of the BIC samples: temperatures, mass Fractions

species	$T_{onset(hc)}$(K)	$T_{shoulder}$(K)	T_{peak}(K)	$T_{offset(l)}$(K)	$Y_{shoulder}$	Y_{peak}
BIC	500	580	625	670	0.72	0.47

3.3.2. Drying and pyrolysis Model

As stated above, BIC combustion is strongly affected by the moisture evaporation phase and volatile pyrolysis phase. The drying phase can be modeled by a reaction, and the volatile matter pyrolysis stage can be explained by one-component mechanisms or three-component reactions mechanisms. In this section, we presented both mechanisms to obtain the kinetic parameters of BIC drying and pyrolysis.

For the mass loss process of each fraction, it is important to solve Eq. (3-16) for each fraction to describe BIC drying and pyrolysis.

$$\frac{\mathrm{dY}_i}{\mathrm{dT}} = \frac{A_i}{\beta} exp(-\frac{E_i}{RT})(1 - Y_i)^{n_i} \quad (3\text{-}16)$$

In Eq. (3-16), $\mathrm{Y}_i = (m_{io} - m_i)/(m_{io} - m_{i\infty})$ is the degree of conversion of the *ith* fraction, β is the heating rate.

In TG analysis, the sample weight (m) is recorded and the overall conversion (Y) is defined as

$$\mathrm{Y} = (m_o - m)/(m_o - m_\infty) \quad (3\text{-}17)$$

In Eq. (3-17), m_0 is the initial sample weight, and m_∞ is the weight of the sample when decomposition of organic material terminated. Meanwhile, the weight of the sample is also the sum of weights of each individual fraction, as shown in In Eq. (3-18)

$$m_0 - m = \sum_i m_{i0} - \sum_i m_i = \sum_i (m_{i0} - m) = \sum_i Y_i (m_{i0} - m_{i\infty}) \quad (3\text{-}18)$$

So, overall conversion can be shown in another way as Eq. (3-19),

$$\mathrm{Y} = \frac{\sum_i Y_i (m_{i0} - m_{i\infty})}{m_0 - m_\infty} = \sum_i r_i Y_i \quad (3\text{-}19)$$

Here $r_i = (m_{io} - m_{i\infty})/(m_o - m_\infty)$, explained as the yield of fraction *i* and $\sum_i r_i = 1$, reflecting the ratio of the mass loss of fraction *i* to the total mass loss during the decomposition process.

So the overall rate of conversion can be expressed as:

$$\frac{\mathrm{dY}}{\mathrm{dT}} = \sum_i \frac{\mathrm{dY}_i}{\mathrm{dT}} = \sum_i r_i \frac{A_i}{\beta} exp(-\frac{E_i}{RT})(1 - Y_i)^{n_i} \quad (3\text{-}20)$$

In Eq. (3-20), 1-Y_i can be explained by the Coats-Redfern equation [62]:

$$\ln\left[\frac{g(Y)}{T^2}\right] = \ln\frac{AR}{\beta T}\left[1 - \frac{2RT}{E}\right] - \frac{E}{RT} \quad (3\text{-}21)$$

In Eq. (3-21), $g(Y)$ is expressed by $g(Y) = \int_0^Y dY/f(Y)$. If n=1, $g(Y) = -In(1 - Y)$, if $n \neq 1$, $g(Y) = (1 - (1 - Y)^{1-n})/(1 - n)$. Then, Eq. (3-20) can be rewritten as:

$$n = 1 \ : \ \frac{\mathrm{dY}}{\mathrm{dT}} = \sum_i r_i \frac{A_i}{\beta} \mathrm{e}^{-E_i/RT} e^{-A_i RT^2/\beta E_i (1-(2RT/E_i))} \exp(-E_i/RT)$$

$$n \neq 1 \ : \ \frac{\mathrm{dY}}{\mathrm{dT}} = \sum_i r_i \frac{A_i}{\beta} \mathrm{e}^{-E_i/RT} \left[1 - \frac{A_i RT^2}{\beta E_i}(1 - n_i)(1 - \frac{2RT}{E_i}) e^{-E_i/RT}\right]^{n_i/1-n_i} \quad (3\text{-}22)$$

The determination of the kinetic parameters for drying and pyrolysis of each organic material were obtained by achieving the minimum of S_{DTG} coefficient of the all experimental data (*T* and *dY/dT*).

$$\mathrm{S}_{DTG} = \sum_{exj} S_{exj} = \sum_{exj} \sum_x [(dY/dT)^{ex} - (dY/dT)^{ca}]^2 \quad (3\text{-}23)$$

Where the superscripts of "*ex*" and "*ca*" are the experimental and calculated results, *exj* is the number of experimental curves, and *x* is the number of data points of each experimental curve. The minimization of $\mathrm{S}_{\mathrm{DTG}}$ was implemented by the Levenberg-Marquardt nonlinear fitting

algorithm [63].

Scheme 1 (One-component mechanisms)

$$w \rightarrow g_w$$

$$v \rightarrow g_v$$

In Scheme 1, BIC pyrolysis was depicted by one-component mechanisms, where *w* is moisture content, *v* is volatile matter and *g* is gas vapors.

The kinetic parameters obtained by Scheme 1 are shown in Table 3.2, we used first order reaction mechanism to depict the drying and pyrolysis reactions, for pyrolysis reaction, we assumed there was only one component, and after pyrolysis reaction, it became the gas.

Table 3. 2 Kinetic parameters of each reaction in Scheme 1 for BIC pyrolysis

	Moisture	volatile
A (s^{-1})	5.13×10^6	3731.6285
E (J/mol)	107672.7750	73403.7318
n	1	1
r	0.1	0.7

Figure 3.8 shows the experimental and calculated (based on one-component mechanisms) DTG curves at a heating rate of 5 K/min, the agreement of experimental and calculated DTG curves about moisture part was pretty good, however, about volatile matter part, it shows obvious discrepancy between the experimental and calculated curves, especially the shoulder region, which proves again the decomposition of volatile matter consists several independent reactions.

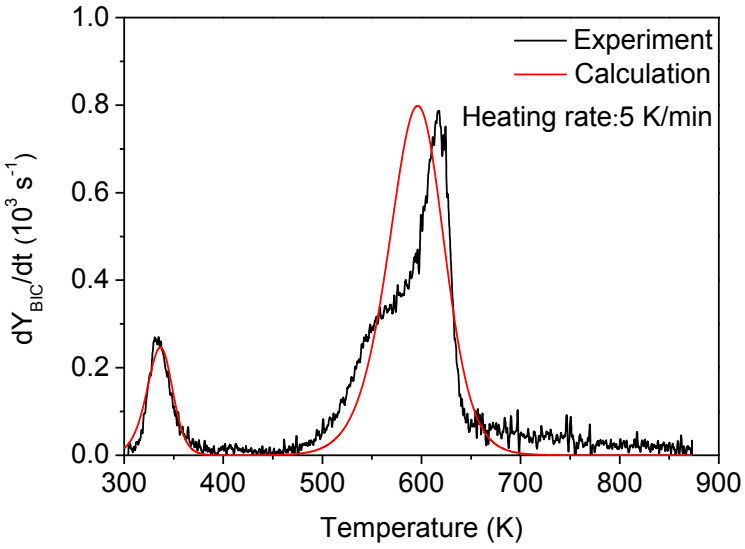

Fig.3. 8 Experimental and simulated DTG curves (scheme 1) for BIC drying and pyrolysis in nitrogen at a heating rate of 5 K/min

Scheme 2 (Three-component mechanisms)

Since it was difficult to reproduce the volatile reaction accurately, especially for the shoulder region in the DTG curve, by one-component mechanisms, therefore, the decomposition can be simulated using three-component mechanisms in BIC: moisture (*w*), hemicellulose (*hc*), cellulose (*ce*), and lignin (*l*). Each fraction processes thermal evaporation/decomposition independently. The overall pyrolysis of BIC is the sum of individual processes.

$$w \rightarrow g_w$$

$$hc \rightarrow g_{hc}$$

$$ce \rightarrow g_{ce}$$

$$l \rightarrow g_l$$

In Scheme 2, BIC pyrolysis was depicted by three-component mechanisms, where *w* is

moisture, *g* is gas vapors. Since the kinetic parameters for drying reaction by Scheme 1 is able to reproduce the DTG curve well, in present part, we only focused on the kinetic parameters of pyrolysis.

The kinetic parameters obtained by Scheme 2 are shown in Table 3.3, we used first order reaction mechanism to depict the drying and pyrolysis reactions, for pyrolysis, we assumed cellulose, hemicellulose and lignin are the main components for the volatile content, according to calculation result, cellulose accounts for 24% of the total mass, hemicellulose is 26% and lignin is 20%.

Table 3. 3 Kinetic parameters in Scheme 2 for BIC drying and pyrolysis

	Moisture	Hemicellulose	Cellulose	Lignin
A (s^{-1})	5.13×10^{6}	752615.6488	2.61×10^{18}	0.1202
E (J/mol)	107672.7750	95116.7637	249163.6075	27932.6739
n	1	1	1	1
r	0.10	0.26	0.24	0.20

Figure 3.9 shows the experimental and simulated DTG curves about the volatile matter pyrolysis phase at a heating rate of 5 K/min by means of Scheme 2, the experimental and simulated DTG curves showed good agreement, especially for the shoulder region. The appearance of the shoulder region in DTG curve was mainly due to the rapid decrease of decomposition rate of hemicellulose and fast increase of decomposition rate of cellulose within a narrow range.

From the degradation characteristics of the BIC sample in last section, we obtained some information to judge whether the kinetic parameters by means of three-component mechanisms are reasonable or not. According to the DTG curve from calculation, the

decomposition of hemicellulose started from 485K, the maximum devolatilization rate of hemicellulose was reached when temperature was 575K. As for cellulose, the maximum devolatilization rate of cellulose appeared when temperature reached 635K. As for lignin, the maximum devolatilization rate of cellulose was obtained when temperature reached 665K. It showed they were very close to the temperatures obtained from the degradation characteristics analysis of the BIC sample.

Again, it showed the multi-component mechanisms were able to simulate the decomposition process well.

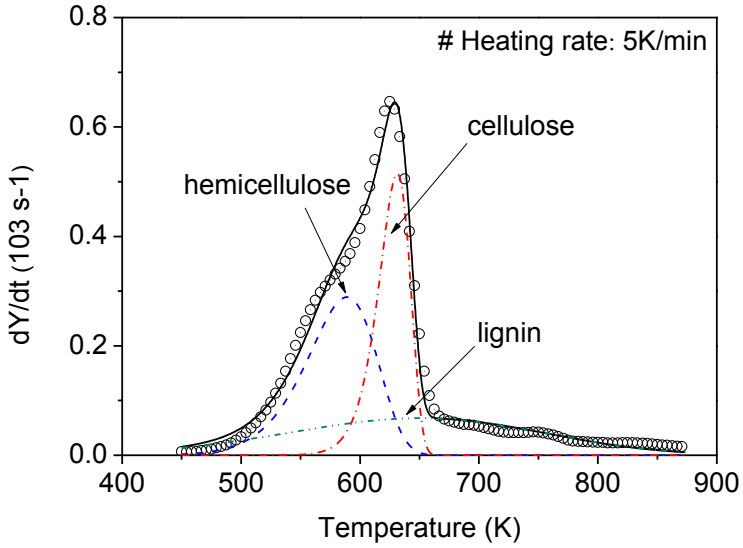

Fig.3. 9 Comparison between the observed (symbols) and simulated differential curves (solid line) for BIC heated at 5 K/min, by three-component devolatilization model.

Here, in present calculation model, we applied the kinetic parameters of drying and pyrolysis reaction from one-component mechanisms. And other thermal parameters and kinetic data used in present calculation model are shown in Table 3.4.

Table 3. 4 Thermal parameters and kinetic data

Parameter	Value	Unit	Ref
A_c	1.2×10^3	m/s	[63]
A_v	3731.6285	1/s	
A_w	5.13×10^6	1/s	
E_c	8.38	J/mol	[63]
E_v	73403.7318	J/mol	
E_w	107672.7750	J/mol	
Q_v	-4.3×10^5	J/kg	[64]
Q_w	-2.7×10^6	J/kg	[54]
Q_c	3.3×10^7	J/kg	[63]
$C_{p,wb}$	$1864 \times (T/300)^{0.406}$	J/kg•K	[65]
$C_{p,db}$	$1764 \times (T/300)^{0.66}$	J/kg•K	[65]
$C_{p,c}$	$1244 \times (T/300)^{0.283}$	J/kg•K	[65]
$C_{p,ash}$	$1219 \times (T/300)^{0.315}$	J/kg•K	[65]
$C_{p,g}$	1100	J/kg•K	[66]
λ_{wb}	$0.196 \times (T/300)^{0.185}$	W/m•K	[65]
λ_{db}	$0.186 \times (T/300)^{0.594}$	W/m•K	[65]
λ_c	$0.065 \times (T/300)^{0.435}$	W/m•K	[65]
λ_{ash}	$0.058 \times (T/300)^{0.353}$	W/m•K	[65]

Chapter 4: Steady combustion

In this Chapter, combustion experiments on BIC had been conducted to observe whether quasi-one-dimensional steady combustion can be attained in room temperature air flow. Initially, the air was metered as 9.17NL/s (550NL/min) and subsequently heated (873 K) by the air supply system and blown onto the bottom surface of the BIC sample, after the bottom face of the BIC sample ignited, the air temperature was switched to room temperature. This experiment was conducted three times under each air flow rate condition, which were 5.83, 7.50, 9.17, 10.83 and 12.50 NL/s (350, 450, 550, 650 and 750 NL/min). Here, NL means litre under normal condition(273K,1 atm).

4.1 Combustion behavior of BIC in convective flow

A direct image of quasi-one-dimensional combustion is shown in Fig. 4.1. Surface combustion was observed at the bottom surface of the BIC sample. However, during any experiment no visible flame was found in the gas phase because of the large stretch rate near the stagnation point. Hence, only smoldering happened.

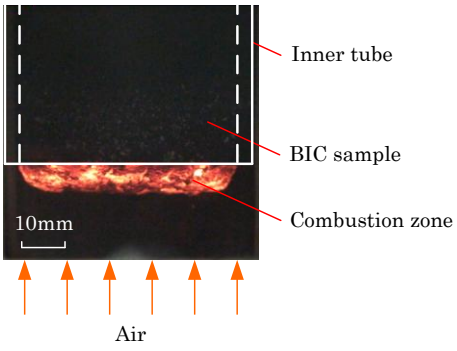

Fig.4. 1 Direct image of end-face combustion

Figure 4.2 illustrates the end face of BIC from IR camera, both before and after the ignition when air flow rate is 12.50 NL/s, before ignition, preheated air was supplied to the bottom surface of BIC, the bottom surface soon was heated up (Fig. 4.1(a)), then the bottom surface was ignited by the preheated air and surface temperature increased to around 1000K (Fig. 4.1(b)), so IR camera can be used to tell whether combustion happen or not.

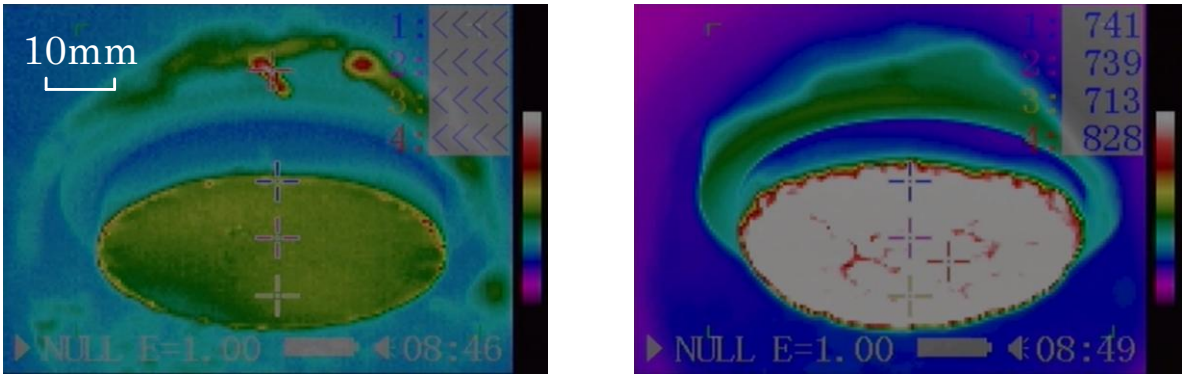

(a) Before ignition

(b) After ignition

Fig.4. 2 Images of end face of BIC from IR camera (Air flow rate: 12.50 NL/s, air temperature (a): 873K; (b): 300K)

4.2 Steadiness of BIC combustion

Temperature histories inside the BIC sample with 12.50 NL/s air flow are shown in Fig. 4.3 as a function of elapsed time. Here elapsed time started from ignition moment. The temperature measurement was conducted with thermocouples set at different depths of the BIC sample, as described in Chapter 3. At any measuring point, the temperature increased gradually to 373 K and maintained at 373 K for a while. This change in temperature could be explained by the moisture content in the BIC sample after the conductive supply from the combustion zone. Subsequently, the temperature quickly increased to 800–1000 K when the

combustion zone came closer to the position of the individual thermocouples. The time to reach the maximum temperature indicated the moment the combustion front arrived at the thermocouple position. Using this information, the propagation characteristics of the combustion zone can be determined. As shown in Fig. 4.3, the peak temperature for 0.03m was quite low, which was due to large fragment of BIC near the thermocouple dropped during the experiment.

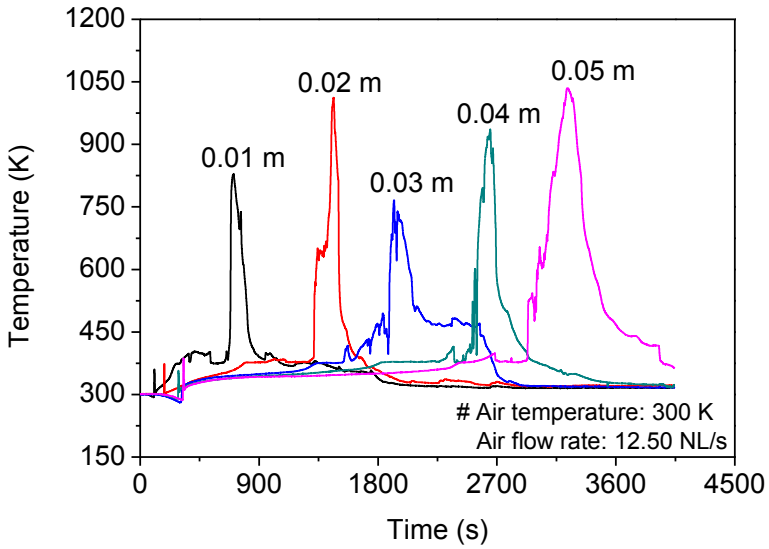

Fig.4. 3 Temperature history inside the BIC sample (Air temperature: 300K, air flow rate: 12.50NL/s)

Temporal changes in the location of the combustion zone and displacement of the combustion front from the initial position are shown in Fig. 4.4 as a function of elapsed time. The air flow rate was the experimental parameter in the figure. In this study, the displacement rate of combustion front was called the regression rate and was given by the slope gradient in Fig. 4.4. For each air flow rate case, we conducted three repeated tests. Plots of Fig. 4.4 were the average of repeated tests. Under high air flow rate conditions (9.17– 12.50 NL/s), quasi-

one-dimensional steady combustion was observed in all repeated tests. The location of the bottom surface varied almost linearly, which indicated that the regression rate was almost constant and larger as the air flow rate increased. In contrast, extinction was always observed before all parts of the BIC sample were consumed under low air flow rate conditions (5.83 NL/s). As for 7.50 NL/s case, in one experiment, extinction happened, while it survived in other two experiments. The regression rate in low air flow rate conditions was smaller than that in high air flow rate conditions. Based on these results, a minimum air flow rate between 5.83 and 7.50NL/s existed, which can sustain steady combustion.

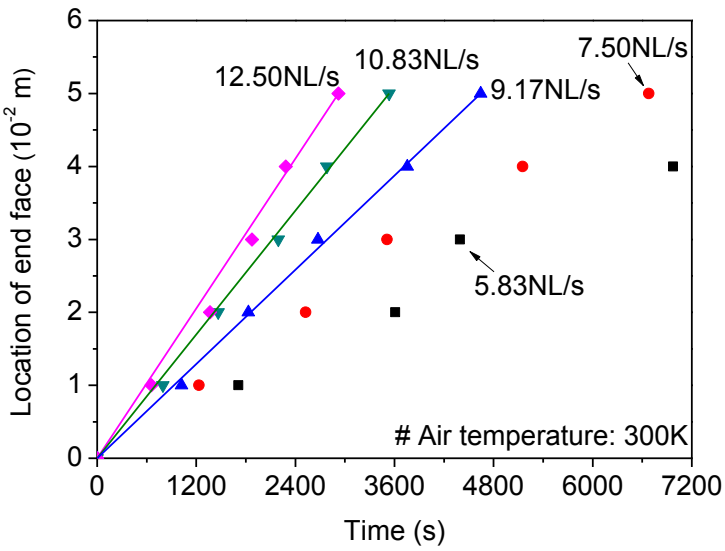

Fig.4. 4 Temporal change of the end-face location (Air temperature: 300K)

From the above observation, steady combustion can be attained under high air flow rate conditions. However, this was not possible under low air flow rate conditions. So there was a critical air flow rate sustaining the steady combustion, in the following section, the mechanism for determining the criteria for steady combustion was discussed on the basis of comparison between calculation and experimental results.

4.3 Dependence of air flow rate on regression rate

The effect of air flow rate on regression rate is shown in Fig.4.5. The experimental data were obtained every 0.01m in the combustion zone. The regression rate increased as the air flow rate increased for both experiments and calculations, of course in the condition extremely close to extinction limit, the effect of chemical part turned to be controlling step, but the general trend in Fig.4.5 was mainly controlled by diffusion process according to the Nusselt number and chemical parameter. In Fig. 4.5, the extinction limit from experiment located between 5.83 NL/s and 6.42NL/s, for calculation, it was also in that range, while the steady combustion can be survived at a flow rate higher than such critical air flow rate. The reason that the calculation results were larger was because of the assumption of a fresh air supply to the bottom surface of the BIC sample. However, the oxygen concentration in the supplied air near the surface may decrease because of oxygen consumption in the gas phase. According to the calculations, the decrease in the regression rate was explained by a decrease in the heat release rate because of a decreased surface temperature. This temperature decrease was the mechanism of extinction because the chemical reaction rate changed nonlinearly, and it suddenly decreased when the regression rate was lower than a critical value.

As discussed in the previous section, the regression rate was controlled by the air flow rate and the combustion was diffusion-controlled. Therefore, there was minimum air flow rate to sustain steady combustion, which would be extensively discussed in the following sections.

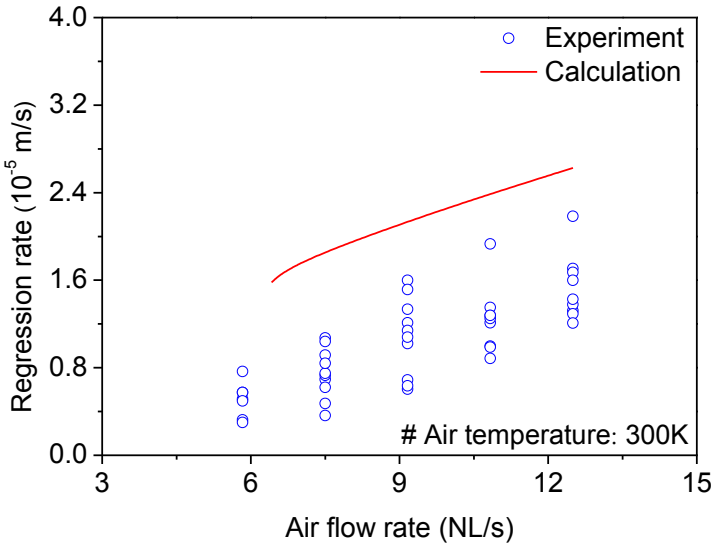

Fig.4. 5 Effect of air flow rate on regression rate (Air temperature: 300K)

4.4 Relationship between the regression rate and combustion zone temperature

Figure 4.6 shows the relationship between regression rate and surface temperature from experiments and calculations. The surface temperature decreases with a decrease in the regression rate for both experiments and calculations. According to the calculations, the decrease in the temperature is explained by a decrease in the heat release rate because of a decreased regression rate, that is, the ratio of heat release to heat loss increases. This temperature decrease is the mechanism of extinction because the chemical reaction rate changes nonlinearly, and it suddenly decreases when the temperature is lower than a critical value.

As discussed in the previous section, the regression rate is controlled by the air flow rate and the combustion is diffusion-controlled. Therefore, there is minimum air flow rate to

sustain steady combustion.

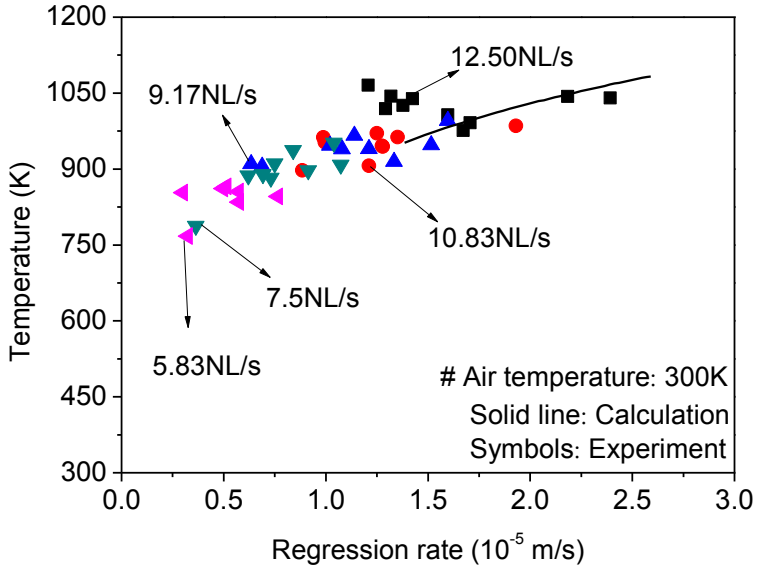

Fig.4. 6 Relationship between regression rate and surface temperature from experiments and calculations

4.5 Effects of BIC density on steady one-dimensional combustion

Figure 4.7 demonstrates the effect of BIC density on regression rate and critical air flow rate. As found in Fig.4.7, when the density of the BIC increased from 900kg/m^3 to1700 kg/m^3, the regression rate, under a certain air flow rate, decreased obviously, which can be explained that when density became larger, it took more time to consume the char, automatically leading to lower regression rate. In Fig.4.7, it shows as density of the BIC increases from 900kg/m^3 to1700 kg/m^3, the critical air flow rate sustaining the steady combustion slightly increases from about 5.75NL/s to around 6.91NL/s, such tendency could be explained as that larger BIC density resulted in more heat loss from the combustion zone to unburned zone,

extinction easily happened.

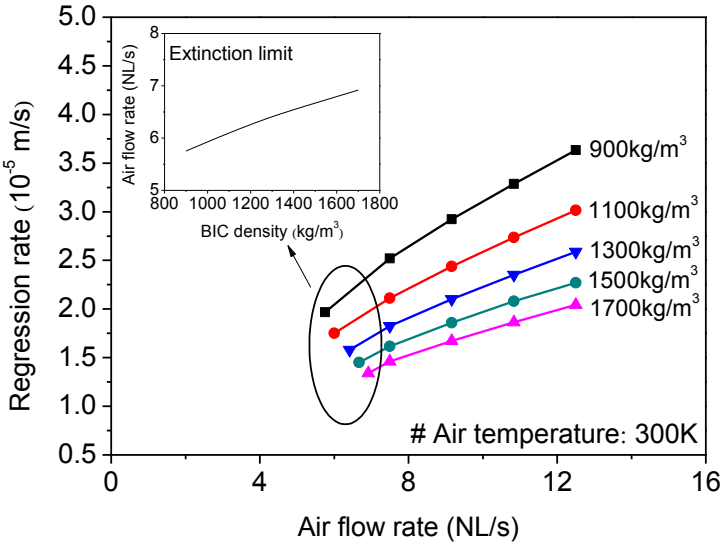

Fig.4. 7 Effect of BIC density on the regression rate and extinction limit (Air temperature: 300K)

4.6 Effects of blowing on steady one-dimensional combustion

The present simulations included Couette model for blowing (see Eq. (3-8)). To investigate the effect of blowing, the calculated regression rate is shown in Fig.4.8 both with and without blowing. It can be seen that the regression rate was higher when blowing was eliminated due to greater diffusion of oxygen to the combustion zone. Blowing also had an appreciable effect on extinction limit, extinction limit without blowing appeared on lower air flow rate than the case including blowing. From Fig.4.8, it also can be concluded that the calculation result with blowing effect was closer to experimental results than the case without blowing.

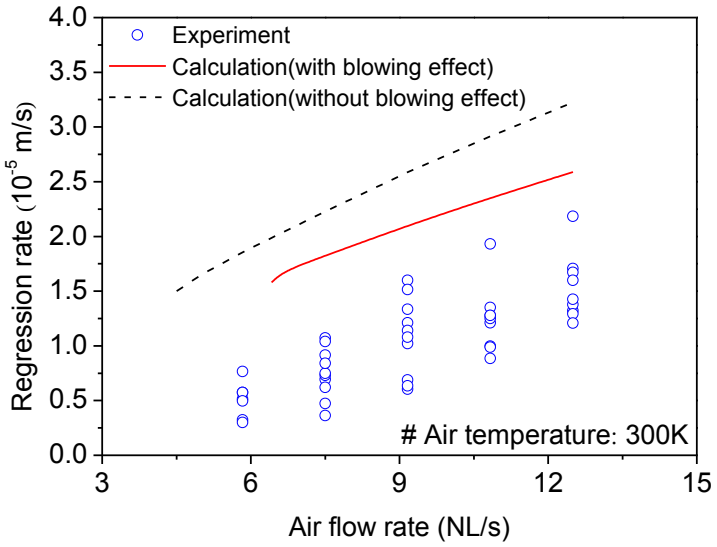

Fig.4. 8 Effect of blowing on regression rate (Air temperature: 300K)

4.6 Concluding remarks

In Chapter 4 experiments with BIC were conducted by burning the BIC quasi-one-dimensionally to observe whether the combustion reaches a steady state in room temperature air flow. In addition, numerical calculations were done to help understand the mechanism that allows for steady combustion and predict the effect of BIC density and blowing. The results thus obtained may be summarized as follows:

(1) It was confirmed that quasi-one-dimensional combustion of BIC was attained in room temperature air flow. The combustion reached a steady state in high air flow rate (9.17NL/s or larger), but extinction was observed in low air flow rate (7.50 NL/s or lower).

(2) According to the numerical calculation, there was a critical regression rate to sustain a steady state. The existence of the critical regression rate was explained by the bottom surface temperature change, which was given by the ratio of heat loss to heat released by char combustion.

(3) A rising tendency of critical air flow rate was observed with the increase of Bio-coke density.

(4) The effect of blowing on extinction limit was investigated. Calculation result with blowing effect was closer to the experimental results than the case without blowing.

Chapter 5: Transient combustion

Chapter 4 showed that steady combustion could be obtained and the minimum regression rate to sustain steady combustion was discussed. However, before steady combustion was reached, the fuel goes through a transient combustion period, and in this phase, the regression rate was not stable. Considering the importance of steady combustion, this transient combustion is an important research topic, which has not been extensively investigated in our previous study. It also allows us to gain a better understanding of the combustion characteristics of this novel biomass fuel and the design of a combustion furnace.

Since it showed steady combustion can be obtained in room temperature air flow, therefore, in the present study, the BIC sample was ignited by preheated air at a temperature of 873 K and an air flow rate of 9.17 NL/s (550 NL/min). After ignition, the air temperature was reduced to 400 K, whereas the flow rate was kept at 9.17 NL/s (550 NL/min), end-face combustion in the transient period between ignition and steady combustion had been investigated. A one-dimensional numerical model was established to study the change of regression rate and temperature distribution in BIC samples placed in opposed convective air flow and compared with experimental findings. Moreover, the mechanism for controlling the transient characteristics of BIC end face combustion and the role of the various parameters in the transient combustion stage was investigated.

5.1 Experimental results

The temperatures inside the BIC sample when air temperature is 400 K are shown in Fig. 5.1 as a function of elapsed time from the point of ignition. Three repeated experiments had

been done and the result in Fig. 5.1 is one individual case of the three. At each measuring point inside the BIC, the temperature increased gradually to and held around 373 K for a while. This is explained by the moisture content in the BIC sample reacting to the conductive heat supply from the combustion zone. Subsequently, the temperature quickly increased to approximate 1000 K as the combustion zone came closer to the individual thermocouples. The maximum temperature was reached when the combustion zone arrived at the thermocouple position. From the data, the propagation characteristics of the combustion zone can be determined. The temperature peak at 0.04 m was comparatively low owing to a large fragment of BIC near the thermocouple dropping off.

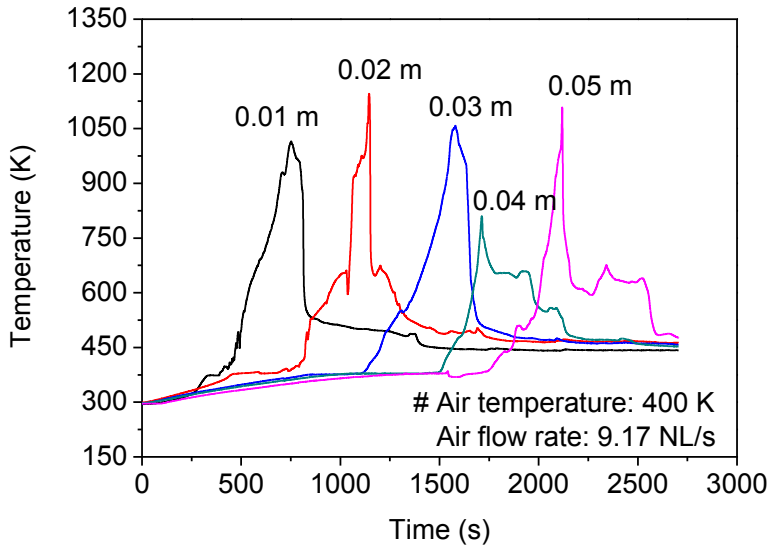

Fig.5. 1 Temperature history inside the BIC sample (Air temperature: 400K, air flow rate: 9.17NL/s)

Temporal changes in the location of the combustion zone and the displacement of the combustion front from its initial position, as shown in Fig. 5.2, is a function of elapsed time, 0 for axis of time means the BIC end face ignition moment. Each plot in Fig. 5.2 is an

averaged data of three repeated experiments, $t_{ave,ni} = \left(\sum_{exi=1}^{3} t_{exi,ni}\right)/3$, the subscript *ave* is the averaged value, *exi* is one of three repeated experiments (*exi* =1,2,3), *ni* is the number of thermocouple (*ni*=1,2,3,4,5), then the error bar was given in the following way: for the minus part of error bars, $minus_{ni} = \min\{(t_{ex1,ni} - t_{ave,ni}), (t_{ex2,ni} - t_{ave,ni}), (t_{ex3,ni} - t_{ave,ni})\}$, for the plus part of error bars, $plus_{ni} = \max\{(t_{ex1,ni} - t_{ave,ni}), (t_{ex2,ni} - t_{ave,ni}), (t_{ex3,ni} - t_{ave,ni})\}$. It shows that in Fig. 5.2, for the first 0.01m, from ignition moment, it takes around 750s, whereas after that, the time taking for the every 0.01m became almost steady and much less than that in the first 0.01m. In this study, the displacement rate of the combustion zone was called the regression rate and is given by the slope gradient shown in Fig. 5.2. It can be seen from Fig. 5.2 that two different regression rates exist. After 0.01 m, the displacement rate of the combustion zone was almost linear and higher than that in the first 0.01 m. Before reaching the steady regression state, a transient propagation period exists.

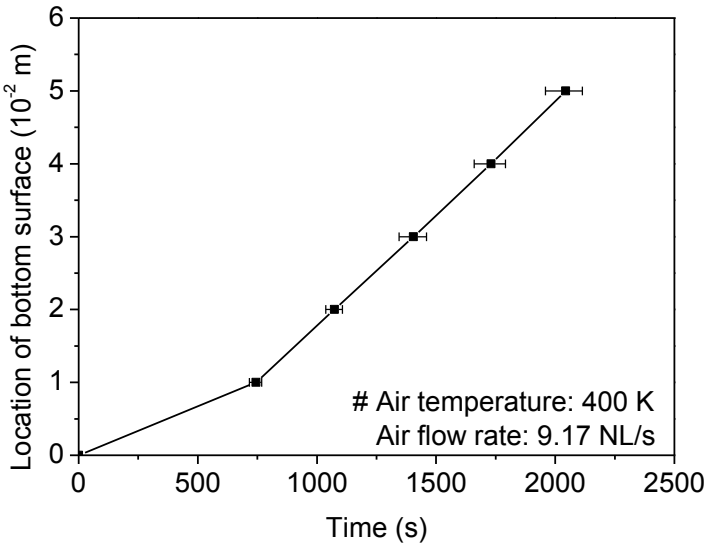

Fig.5. 2 Temporal changes of the end-face location (Air temperature: 400K, air flow rate: 9.17NL/s)

5.2 Calculation results

To better understand this transient combustion region and investigate the role of the various parameters, we compared the results of a numerical simulation with these experimental results.

5.2.1 Transient combustion behavior of BIC

Figure 5.3 illustrates the regression rate of BIC during combustion in the experiment and the model. Every point of the experimental regression rate represents the average regression rate over every 0.01 m. Since we repeated the experiment three times, for every 0.01m BIC length, we have 3 points as shown in Fig.5.3. Before reaching steady combustion, a non-negligible transient combustion region exists both in the experiment and the model. The exact duration of the transient combustion region was difficult to track under experimental conditions, but we conclude that it took less than 750 s to achieve steady combustion; while in the model, the transient period lasted around 650 s. The numerical model defined the steady combustion region when $(rr_t - rr_{t-1})/rr_{t-1} < rtol$, where rr_t and rr_{t-1} are the regression rates at two consecutive time steps, and $rtol$ is the relative tolerance, we set it as 0.005. A difference exists between the calculated and 0-0.01 m regression rates measured in the experiment. This is due to the fact that single-step char oxidation is insufficient to fully describe the complex char reaction. However, both the experiment and model confirm the appearance of the transient combustion period and yield qualitatively similar descriptions of it.

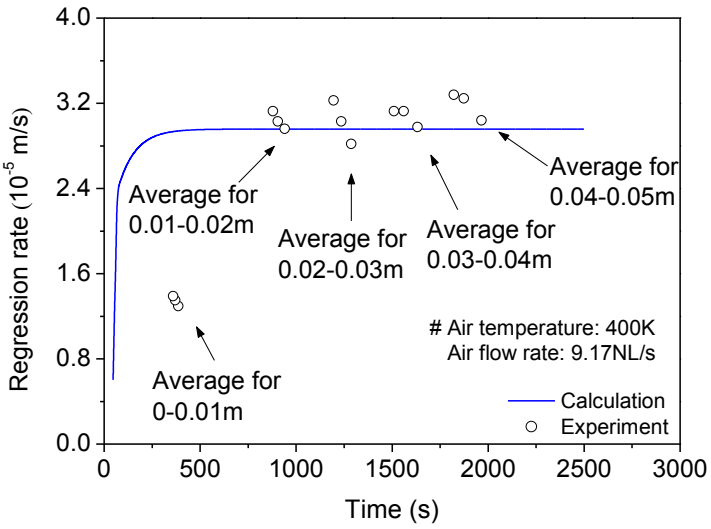

Fig.5. 3 Combustion behavior of BIC in convective air flow (Air temperature: 400K, air flow rate: 9.17NL/s)

5.2.2 Effect of volatile matter content on the transient combustion of BIC

Next, we focused on the effect of the volatile content of the BIC on combustion behavior. When varying the volatile content of the BIC, the moisture content accounted for 10% of the total mass, whereas the remaining parts were allocated to char and ash in the ratio of 13:7. As is shown in Fig. 5.4, in every case, the regression rate can be divided into two distinct regions: a transient region (dashed line) and a steady regression region (solid line), black dots show the boundary of transient region and steady regression region. We omitted calculation data at very initial moment of the combustion for figure drawing in this paper in order to avoid overcrowding. The regression rate increased in both regions with the volatile content of the BIC. This was because the increased volatile matter in the BIC resulted in a reduction in the other contents such as char, which produced a larger regression rate. The duration of the transient regression period decreased as the volatile content increased.

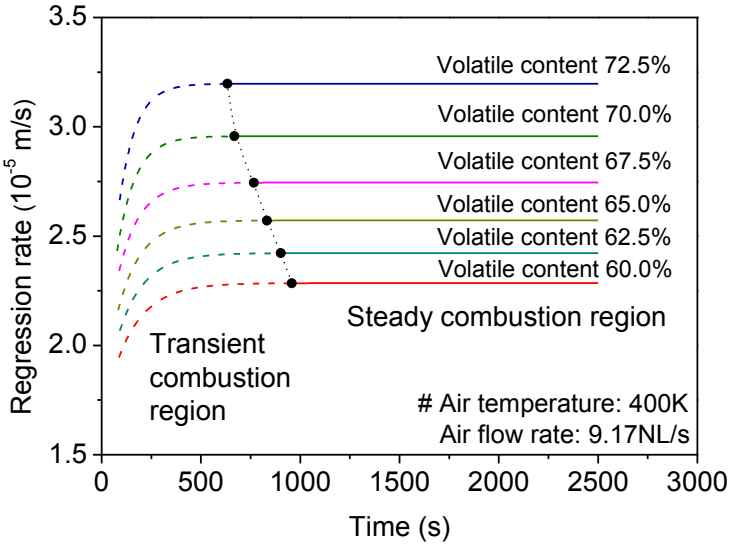

Fig.5. 4 Time-dependent regression rate at different volatile content levels (Air temperature: 400K, air flow rate: 9.17NL/s)

To understand this tendency, we need to consider the evolution of the temperature distribution inside the BIC. It is known that the key to steady combustion is a steady temperature distribution inside the BIC. The duration of transient regression period depends on the time taken to move from the initial temperature distribution to the final steady temperature distribution. The predictions of the process dynamics for the time-dependent temperature distribution, regression rate, and propagation rate of the decomposition and drying fronts with a volatile content of 60.0% are given in Figs. 5.5 and 5.6. Owing to the short ignition delay time (approximately 60 s), only a thin layer of BIC was heated. At the point where the air temperature was switched from 873 to 400 K, the initial temperature distribution inside the BIC was steep and surface temperature was relatively low (Fig. 5.5). The propagation rate of the drying and decomposition fronts could easily exceed the surface regression rate (Fig. 5.6). As can be seen from Fig. 5.5, 120 seconds after the switch, the

drying and decomposition fronts propagated into the deeper parts of the BIC. This made the gradient of temperature distribution less steep and increased the surface temperature. Over time, the difference between the regression and propagation rates of the drying and decomposition fronts became less evident (Fig. 5.6). The time progression of temperature distribution became less obvious by 360–480 seconds after the switch (Fig. 5.5). Finally, as the surface temperature increased further, the regression rate caught up with the propagation rate of the drying and decomposition fronts. Thus, a steady temperature distribution was obtained, and a steady combustion was achieved.

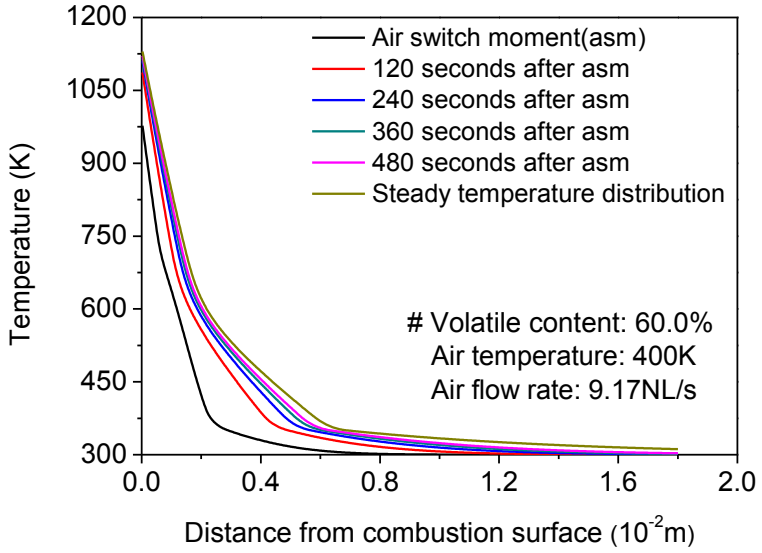

Fig.5. 5 Time-dependent temperature distribution inside BIC (Air temperature: 400K, air flow rate: 9.17NL/s, Volatile content=60.0%)

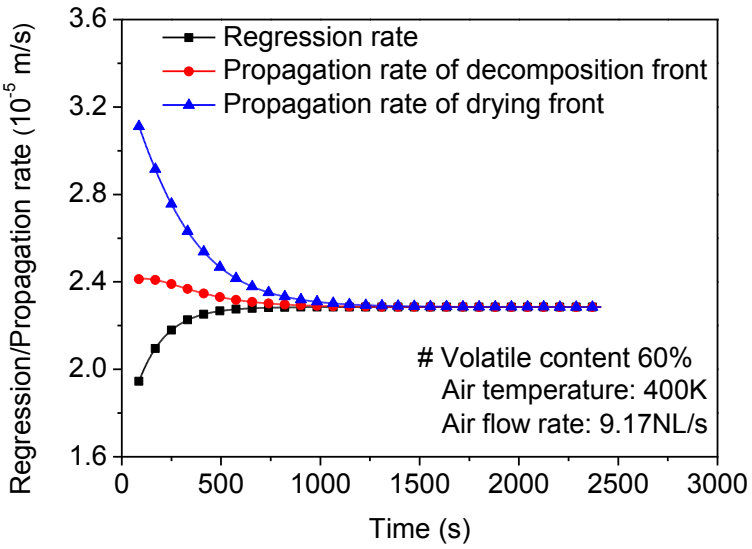

Fig.5. 6 Time-dependent regression rate and propagation rate of decomposition and drying fronts (Air temperature: 400K, air flow rate: 9.17NL/s, volatile content=60.0%)

This suggests that the final steady temperature distribution and propagation rate of the temperature distribution inside BIC are the key factors that determine the duration of the transient combustion phase. The final steady temperature distribution at different volatile contents is given in Fig. 5.7. We defined the final steady temperature distribution as the distribution when the regression rate and the propagation rates of the decomposition and drying fronts were the same. The results suggest that a lower volatile content in the BIC results in a deeper propagation of the drying and decomposition fronts. Meanwhile, we investigated the propagation rate of the temperature distribution inside BIC at different volatile contents. The time-dependent propagation rate of the drying front at different volatile contents, as shown in Fig. 5.8, suggests that the propagation rate of the drying front increases with the volatile content inside the BIC. This explains why the lower volatile content case has a longer transient combustion region with a deeper temperature distribution inside the BIC and a lower temperature propagation rate.

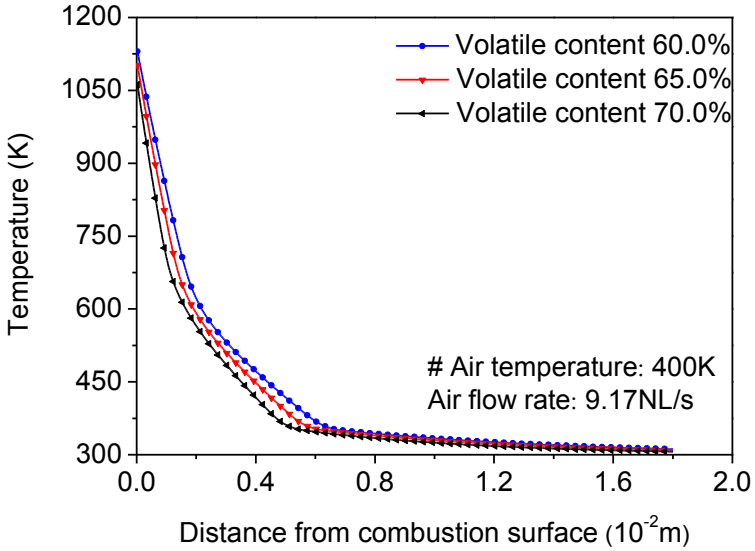

Fig.5. 7 Steady temperature distribution inside BIC at different volatile content levels (Air temperature: 400K, air flow rate: 9.17NL/s)

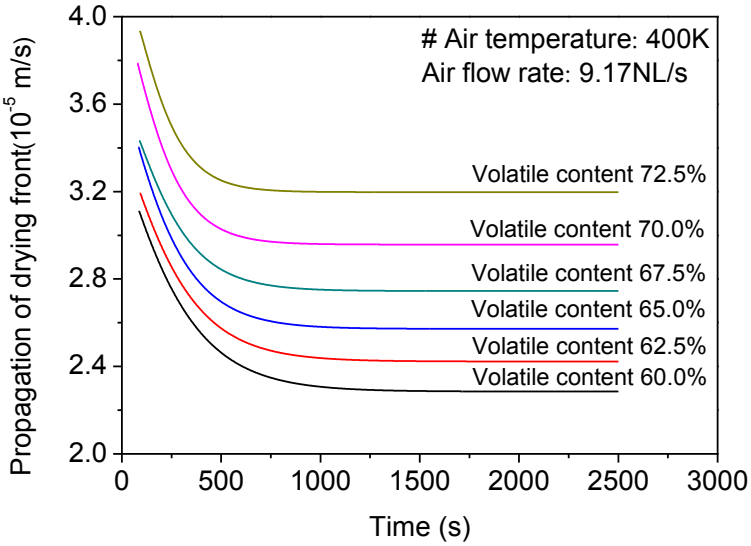

Fig.5. 8 Propagation rate of drying front at different volatile content levels (Air temperature: 400K, air flow rate: 9.17NL/s)

5.2.3 Effect of moisture content on the transient combustion of BIC

When varying the moisture content of the BIC, the volatile content accounted for 70.0%

of the total, whereas the remainder was treated as char and ash in the ratio of 13:7. As shown in Fig. 5.9, the moisture content had a similar influence on BIC combustion behavior as the volatile content level. The regression rate increased in both the transient and steady regions with the moisture content, for the same reasons as stated for the volatile content. A lower moisture content produced a longer transient regression period. As in the analysis of the effect of volatile content, the final steady temperature distribution and propagation rate of the temperature distribution inside the BIC were the key factors. Figure 5.10 shows the different final steady temperature distribution inside the BIC at different moisture content levels. It was found that both the decomposition and drying fronts penetrated deeper into the BIC as the moisture content of the BIC increased. A lower moisture content is favorable for the penetration of the drying front, and a mild temperature gradient achieves a balance between the conduction heat and the heat available for evaporation. At a higher moisture content of 12.5%, the large heat sink retards the propagation of the drying front compared with that in the 5.0% case. A steep temperature gradient formed to support the large amount of heat was used for evaporation. Fig. 5.11 shows the propagation rate of the drying front at different moisture content levels. The propagation rate of the drying front increased with the moisture content. This explains why a lower moisture content resulted in a longer transient combustion period.

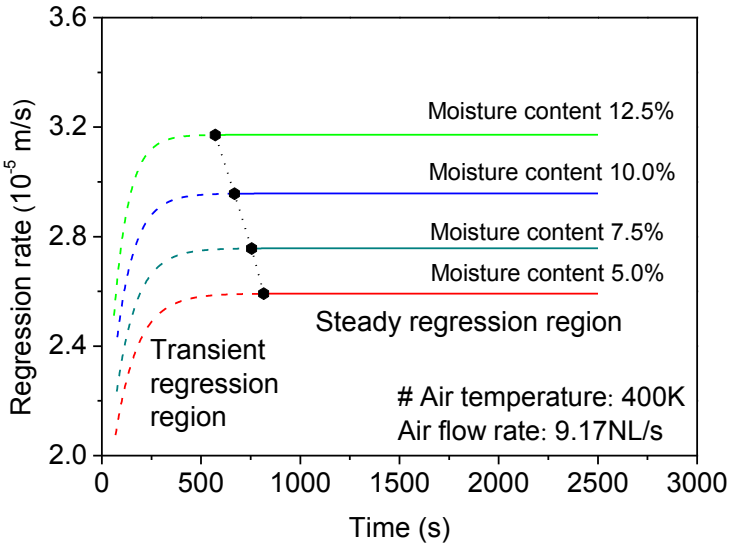

Fig.5. 9 Time-dependent regression rate at different moisture content levels (Air temperature: 400K, air flow rate: 9.17NL/s)

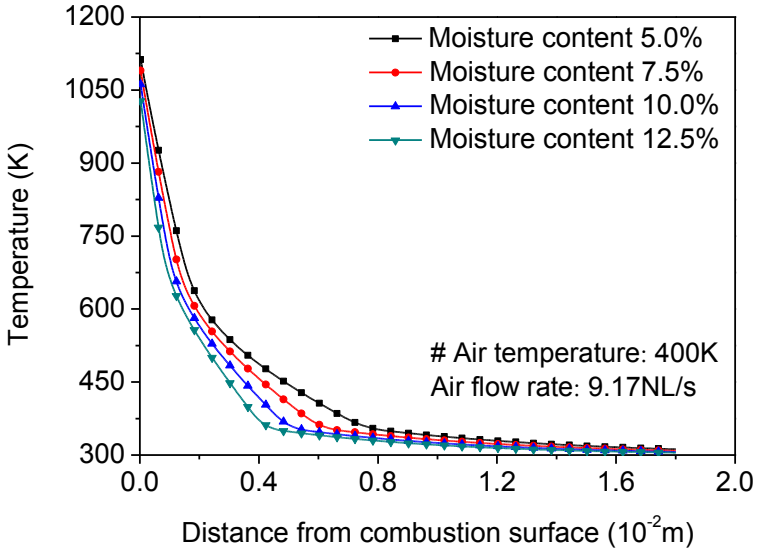

Fig.5. 10 Steady temperature distribution inside BIC at different moisture content levels (Air temperature: 400K, air flow rate: 9.17NL/s)

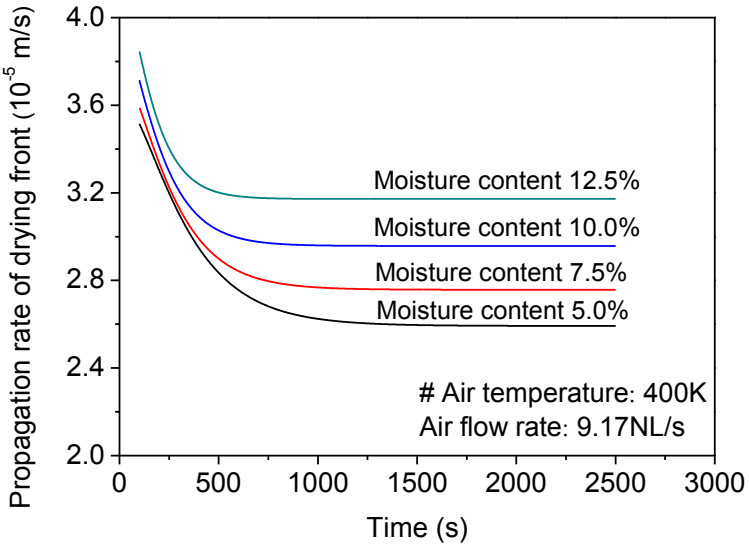

Fig.5. 11 Propagation rate of drying front at different moisture content levels (Air temperature: 400K, air flow rate: 9.17NL/s)

5.2.4 Effect of BIC density on the transient combustion of BIC

Figure 5.12 illustrates the effect of BIC density sample on regression rate and length of transient combustion period. As shown, larger BIC density always obtained smaller regression rate, both in the transient region and steady region, which was due to the increase of char. However, longer transient combustion period was shown for larger BIC density, as density increased from 989kg/m^3 to 1510kg/m^3, the transient period increased from 530s to around 750s, such tendency was coincident with the negative effect of larger density on the development towards final steady temperature distribution according to energy equation.

According to the same analysis process, we checked the final steady temperature distribution at different BIC density from Fig. 5.13, as can be seen, even though the BIC density increased from 989 kg/m^3 to 1380 kg/m^3, the final steady temperature distribution was barely affected by the density. However, as for the effect of BIC density on the propagation rate of temperature distribution, taking the propagation rate of drying front as an

example, we can see from Fig. 5.14 the larger BIC density always obtained lower propagation rate. That's why larger BIC density had longer transient combustion region.

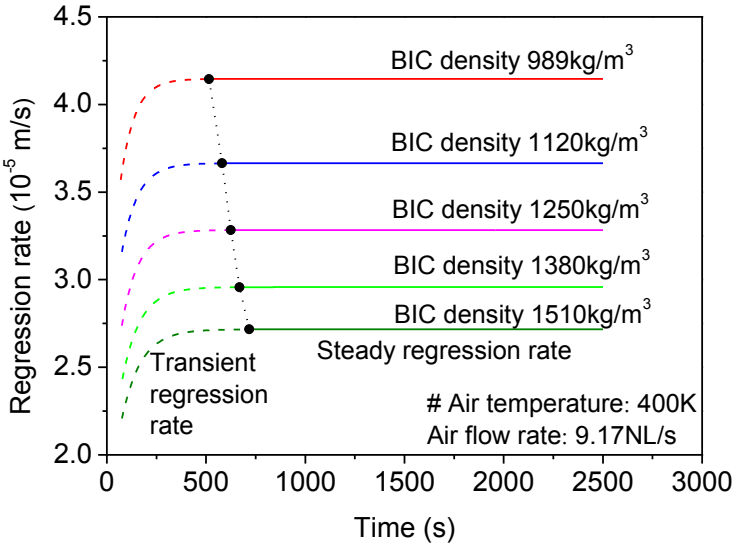

Fig.5. 12 Time-dependent regression rate at different BIC density (Air temperature: 400K, air flow rate: 9.17NL/s)

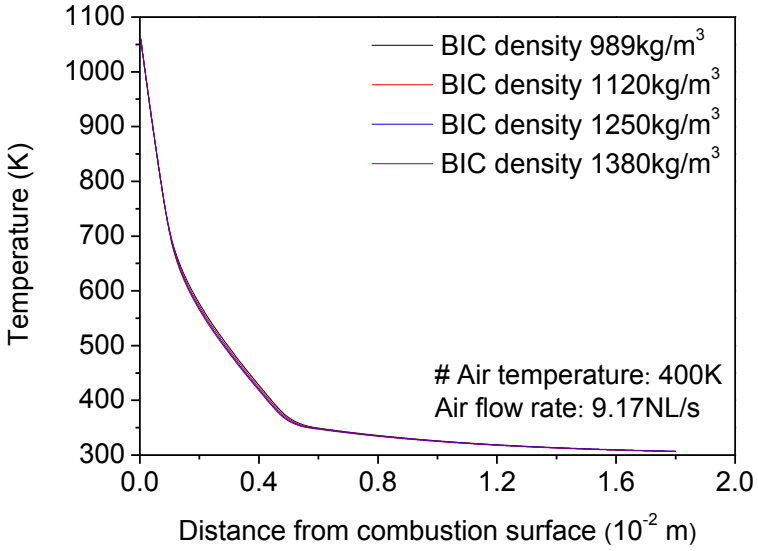

Fig.5. 13 Steady temperature distribution inside BIC at different BIC density (Air temperature: 400K, air flow rate: 9.17NL/s)

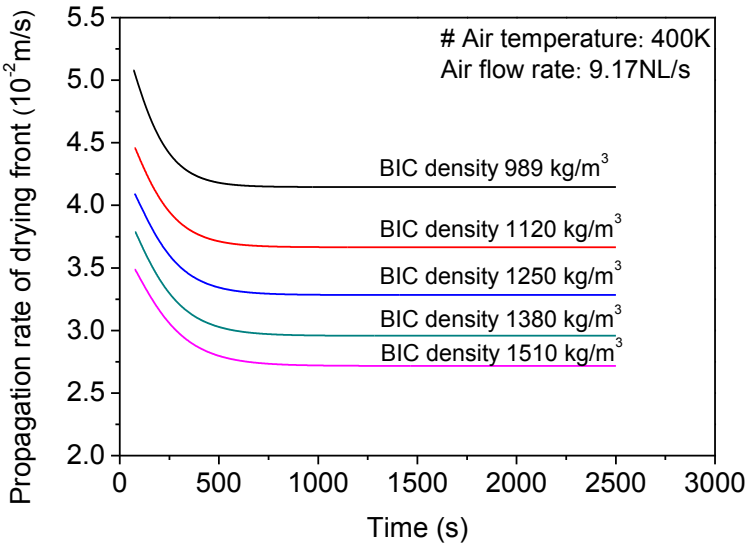

Fig.5. 14 Propagation rate of drying front at different BIC density (Air temperature: 400K, air flow rate: 9.17NL/s)

5.2.5 Effect of air flow rate on the transient combustion of BIC

It illustrates the relation between the time of transient combustion period and moisture content at different air flow rate in Fig. 5.15. For each air flow rate, just as the discussion in last section, the duration of transient combustion period decreased as the moisture content increased. However, as the air flow rate decreased, duration of transient combustion period increased, as for this tendency, taking moisture content 5.0%, volatile content 70.0% case as example, we checked the steady temperature distribution under different air flow rate (Fig. 5.16), the surface temperature increased with air flow rate, which is due to stronger diffusion of oxygen, however the location of drying front and decomposition front appeared on the deeper part of BIC with lower air flow rate. Meanwhile, it illustrates the time-dependent propagation rate of drying front at different air flow rate in Fig. 5.17, the propagation rate of drying front increased as the air flow rate increased, combining Fig. 5.16 and Fig. 5.17, we

can conclude that it takes more time to achieve the final steady temperature distribution with lower air flow rate.

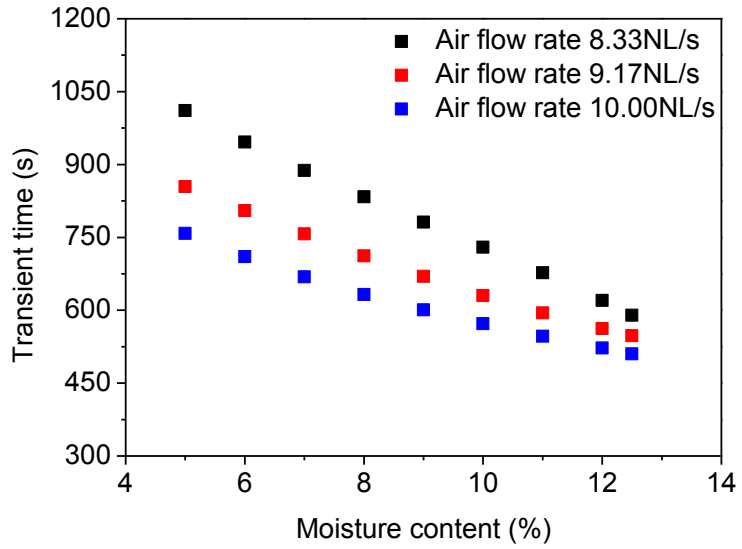

Fig.5. 15 Relation between transient time and moisture content at different air flow rate

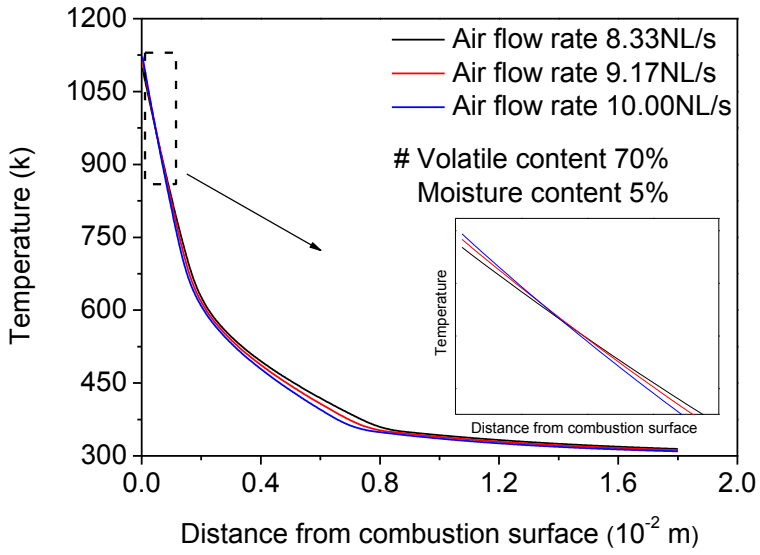

Fig.5. 16 Steady temperature distribution inside BIC at different air flow rate

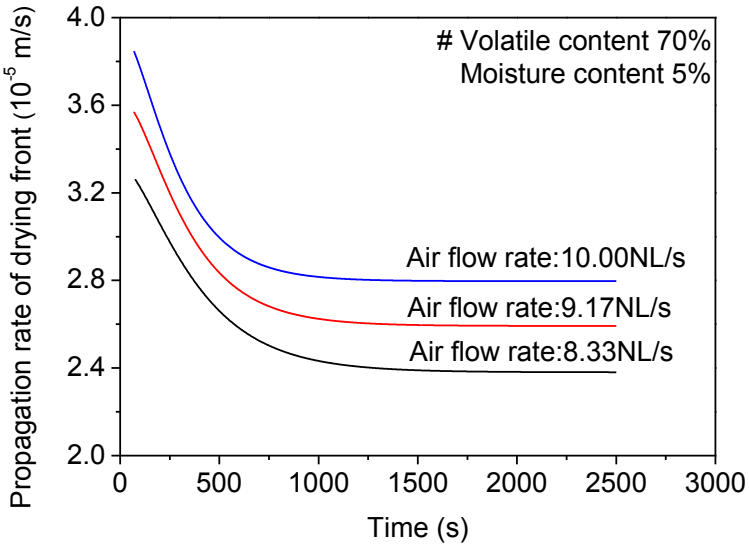

Fig.5. 17 Propagation rate of drying front at different air flow rate

5.2.6 Effect of air temperature on the transient combustion of BIC

As observed in Chapter 4, quasi-steady combustion could be obtained in room temperature air flow. However, in present Chapter, we found that with 400K air flow case, evident transient combustion period appeared. So it is important to investigate the effect of air temperature on transient combustion and why quasi-steady combustion can be obtained in room temperature air flow.

It illustrates the time-dependent regression rate at different air temperature in Fig.5.18. We can find that the regression rate increased in both transient and steady combustion regions with increasing air temperature. This was because the increased air flow temperature resulted in an increase in diffusion coefficient. However, the duration of the transient regression period decreased as the air temperature increased, as the air temperature increased from 300K to 500K, the transient combustion period decreased from around 1000s to less than 500s.

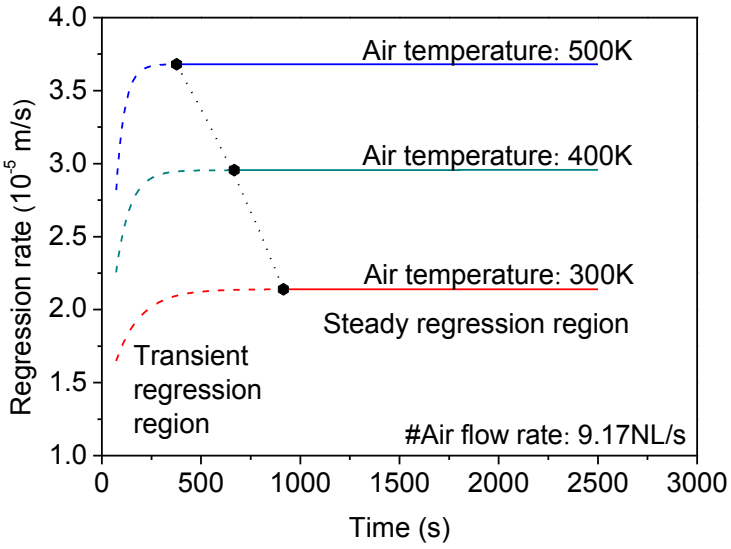

Fig.5. 18 Time-dependent regression rate at different air temperature (Air flow rate: 9.17NL/s)

It seems that this result was contradicted with the conclusion that quasi-steady combustion can be obtained in room temperature air flow in Chapter 4, nevertheless, we need separate two concept: long transient period and evident transient period, long transient time does not mean the evident transient period, it illustrates the average regression rate for every 0.01m under different air flow temperature, 300K, 400k and 500K, respectively, from both experiment and calculation in Fig.5.19(a), (b), (c), we can find that under 300K case, the average regression rate in the first 0.01m was quite similar with following average regression rate, just slightly smaller. However, for the 400K case, the difference of average regression rate between the first 0.01m and following distance became obvious. Moreover, such differences were more evident as air flow temperature became higher. To explain such phenomenon, the ratio between time scale of regression rate to time scale of heat transfer was proposed, the time scale of regression rate was defined as $\delta_{rr} = \delta_{rr,b} - \delta_{rr,f}$, here, δ is symbol of time scale, subscript *rr* is regression rate, *b* is the regression rate just after ignition,

f means the final steady phase, the time scale of heat transfer δ_{ht} was defined as the time duration from initial temperature distribution inside BIC sample just after ignition to reaching the final steady temperature distribution inside BIC sample.

The ratio between time scale of regression rate to time scale of heat transfer δ_{rr}/δ_{ht} can be used to explain whether the transient period is evident or not, in another word, this ratio is used to discuss how difference between the average regression rate in the first 0.01m and the average regression rate in the following distance, larger value of δ_{rr}/δ_{ht} resulted in more evident transient period, simple way to understand such parameter is assuming δ_{ht} is the same for all cases, larger value of δ_{rr}/δ_{ht} means during the same transient combustion time, the increment of regression rate is more prominent, resulting in more evident transient period in the first 0.01m. As shown in Fig.5.19 (d), this ratio became larger as the increase of air temperature, which indicated transient period became more evident under higher temperature case. That explain why quasi-steady-combustion can be obtained under room temperature air flow.

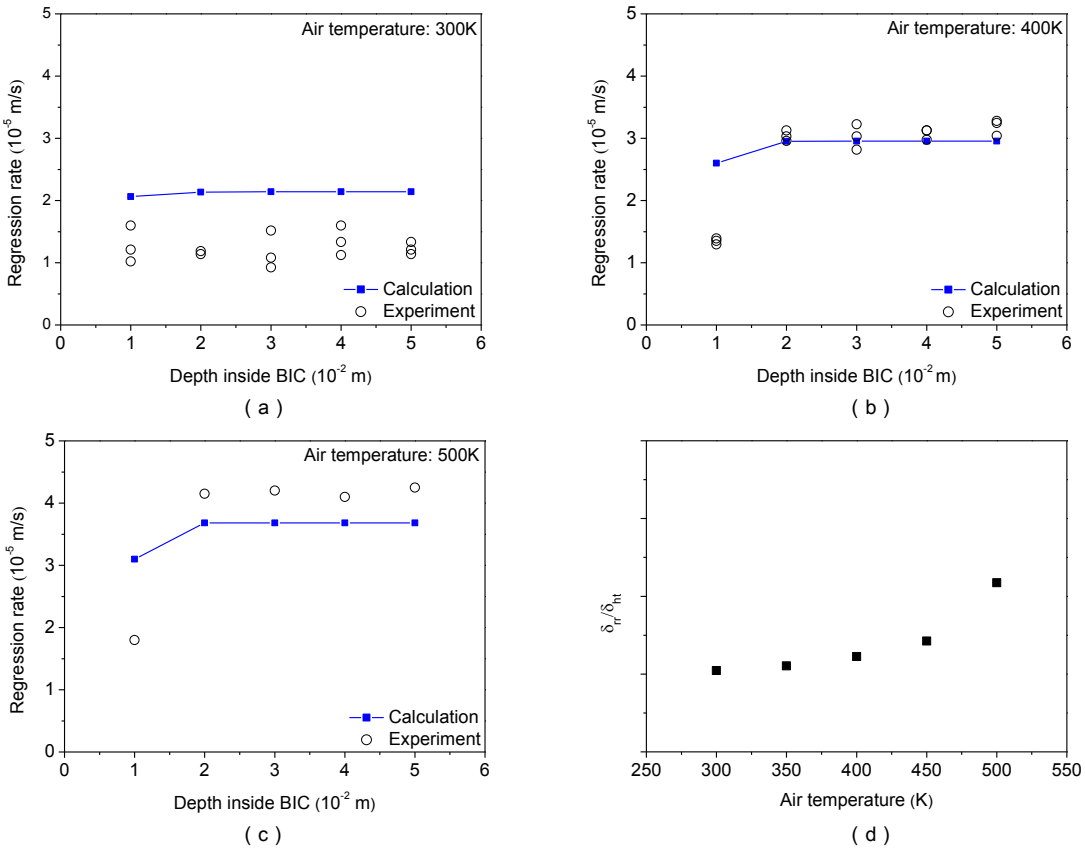

Fig.5. 19 Average regression rate of every 0.01m at different air temperature and the ratio of time scale of regression rate to time scale of heat transfer under different air temperature (Air flow rate: 9.17NL/s)

5.3 Concluding remarks

The transient combustion phase of BIC was investigated in this Chapter both in experiment and calculation, the mechanism controlling the transient combustion was obtained and the effect of moisture contents in BIC, volatile contents in BIC, density of BIC, air flow rate, air temperature on transient combustion behavior were discussed. The results may be summarized as follows:

(1) Before reaching the steady combustion stage, a transient combustion period appeared both in the experiment and model.

(2) The transient combustion was a dynamic process wherein the surface temperature, regression rate, and temperature distribution inside the BIC kept changing.

(3) When the moisture content decreased, the transient combustion period increased. This was because, at a low moisture content, the BIC had a deeply propagated final steady temperature distribution, slowing the evolution from the initial temperature distribution to the final temperature distribution.

(4) The transient combustion period decreased as the volatile content increased. This was because, in the low volatile content case, the final steady temperature distribution propagated deeply, while the evolution rate from the initial temperature distribution to the final temperature distribution was slower.

(5) A rising tendency of transient combustion period was observed with the increase BIC density, BIC density had little effect on the final temperature distribution while it played an important part in the propagation rate of temperature distribution.

(6) Lower air flow rate obtained longer transient combustion period, cause lower air flow rate case always gained deeply propagated final steady temperature distribution and lower propagation rate .

(7) The transient combustion period decreased as the air flow temperature increased. However, transient combustion period became more evident as air flow temperature increased, which was due to the ratio of the time scale of regression rate to the time scale of heat transfer became larger under higher air flow temperature case.

Chapter 6: Summary

End-face combustion experiments and one-dimensional calculations were conducted on cylindrical bio-coke(BIC), i.e., a highly densified biomass briquette, to investigate whether quasi-one-dimensional steady combustion can be attained in forced air flow with different air temperature and air flow rate, as measured by a steady regression rate.

In Chapter 2, we presented the properties of BIC including feedstock, manufacture process, density, elemental analysis, proximate analysis of BIC, and based on the thermogravimetric curves, we obtained the kinetic parameters for drying and pyrolysis by means of one-component mechanisms and multi-component mechanisms, respectively. According to elemental analysis, the main elements of BIC are C (47.72%), H (5.95%), N (0.47%) and Cl and S belong to negligible level. According to proximate analysis, moisture accounts for 10.0% of total mass, volatile content accounts for 70.0%, fix carbon is 13.0% and ash is 7.0%.

In Chapter 3, we presented the experiment setup and the calculation method, and we obtained the kinetic parameters of drying reaction and pyrolysis reaction by means of multi-component mechanisms and one-component mechanisms of primary pyrolysis, respectively. Results show multi-component mechanisms were capable to reproduce the pyrolysis DTG, especially for the shoulder part in DTG curve.

In Chapter 4, experiments with BIC were conducted by burning the BIC quasi-one-dimensionally to observe whether the combustion reached a steady state in room temperature air flow. In addition, numerical calculations were done to help understand the mechanism that allows for steady combustion and predict the effect of BIC density and blowing. The results thus obtained may be summarized as follows: (1) It was confirmed that quasi-one-

dimensional combustion of BIC was attained in room temperature air flow. The combustion reached a steady state in high air flow rate (9.17NL/s or larger), but extinction was observed in low air flow rate (7.50 NL/s or lower). (2) According to the numerical calculation, there was a critical regression rate to sustain a steady state. The existence of the critical regression rate was explained by the bottom surface temperature change, which was given by the ratio of heat loss to heat released by char combustion. (3) A rising tendency of critical air flow rate was observed with the increase of Bio-coke density. (4) The effect of blowing on extinction limit was investigated. Calculation results with blowing effect were closer to the experimental results than the case without blowing.

In Chapter 5, The transient combustion phase of BIC was investigated in this Chapter both in experiment and calculation, the mechanism controlling the transient combustion was obtained and the effect of moisture contents in BIC, volatile contents in BIC, density of BIC, air flow rate, air temperature on transient combustion behavior were discussed. The results may be summarized as follows: (1) Before reaching the steady combustion stage, a transient combustion period appeared both in the experiment and calculation. (2) The transient combustion was a dynamic process wherein the surface temperature, regression rate, and temperature distribution inside the BIC kept changing. (3) When the moisture content decreased, the transient combustion period increased. This was because, at a low moisture content, the BIC had a deeply propagated final steady temperature distribution, slowing the evolution from the initial temperature distribution to the final temperature distribution. (4) The transient combustion period decreased as the volatile content increased. This was because, in the low volatile content case, the final steady temperature distribution propagated deeply, while the evolution rate from the initial temperature distribution to the final temperature distribution was slower. (5) A rising tendency of transient combustion period was

observed with the increase Bio-coke density, Bio-coke density had little effect on the final temperature distribution while it played important part in the propagation rate of temperature distribution. (6) Low air flow rate obtained long transient combustion period, cause low air flow rate case always gained deeply propagated final steady temperature distribution and low propagation rate. (7) The transient combustion period decreased as the air flow temperature increased. However, transient combustion period became more evident as air flow temperature increased, which was due to the ratio between the time scale of regression rate to time scale of heat transfer became larger under higher air flow temperature case.

References

[1] Key World Energy Statistic 2016, http://www.iea.org/publications/freepublications/publication/KeyWorld2016.pdf

[2] M.P. Koh, W. K. Hoi, Biomass Bioenergy 25 (2003) 517–29.

[3] N. Sasaki, W. Knorr, D. R. Foster, H. Etoh, H. Ninomiya, S. Chay, et al, Appl Energy 86 (2009) S140–50.

[4] P. M. Kendry, Bioresource Technol 83(2002) 37–46.

[5] O. Theander, Cellulose, hemicellulose and extractives. In:Overend RP, Milne TA, Mudge LK, editors. Fundamentals of biomass thermochemical conversion. London: Elsevier; 1985.p. 35–60.

[6] W. E. Hillis, Wood and biomass ultrastructure. In: Overend RP,Milne TA, Mudge LK, editors. Fundamentals of biomass thermochemicalconversion. London:Elsevier; 1985. p. 1–33.

[7] W. G. Glasser, Lignin. In: Overend RP, Milne TA, Mudge LK, editors. Fundamentals of biomass thermochemical conversion. London: Elsevier; 1985. p. 61–76.

[8] G. M. Barton, Definition of biomass samples involving wood, bark and foliages. In: Overend RP, Milne TA, Mudge LK, editors. Fundamentals of biomass thermochemical conversion. London: Elsevier; 1985. p. 1137–44.

[9] F. A. Agblevor, S. Besler, A. E. Wiselogel, Energy Fuels 9(1995) 635–40.

[10]D. C. Blasi, G. Signorelli, D. C. Russ, G. Rea, Ind Eng Chem Res 38(1999) 2216–24.

[11]K. Raveendran, A. Ganesh, K. Khilar, Fuel 74(1995) 1812–22.

[12]K. Raveendran, A. Ganesh, K. Khilar, Fuel 74 (1996) 987–98.

[13]B. M. Jenkins, R. R. Bakker, J. B. Wei, Biomass Bioenergy 10(1996) 177–200.

[14]B. M. Jenkins, L. L. Baxter, J. T. R. Miles, T. R. Miles, Fuel Process Technol 54(1998) 17–46.

[15]R. Saidura, E.A. Abdelaziza, A. Demirbas, M.S. Hossaina, S. Mekhilefc, Renewable and Sustainable Energy Reviews 15 (2011) 2262–2289.

[16]H. Yan, O. Fujita, Fuel 15(2017) 595–602.

[17]A. Gungor, Biomass and Bioenergy 34 (2010) 506-514.

[18]D. R. M. Wright, Y. Huang, S. Rezvani, Y. Wang, Fuel 86 (2007) 2032–42.

[19]A. A. Khan, W. D. Jonga, P. J. Jansens, H. Spliethoff, Fuel Process Technol 90(2009) 21–50.

[20]A. Demirbas, Prog Energy Combust Sci 31(2005) 171–92.

[21]W. Ramsay, Energy Policy 4(1985) 326–9.

[22]S. Mizuno, T. Ida, M.F uchihata, K. Kuwana, 6th Int. Symp. Scale Modeling, (2009) on USB memory #1-13.

[23]K. Ishii, H. Murata, K. Kuwana, S. Mizuno, A. Morita, T. Ida, Kouon Gakkaishi 35 (2009) 91–6.

[24]T. Ida, J Jpn Inst Energy 90 (2011) 2–9.

[25]H. Ito, Y. Sakai, T. Ida, Y. Nakamura, O. Fujita, J. Thermal Science and Technology 6 (2011) 111–22.

[26]I. Obernberger, G. Thek, Biomass and Bioenergy 27(2004) 653-69.

[27]T. Nakahara, H. Ito, O. Fujita, Proc. 50th Symposium (Japanese) on Combustion D134 (2012) 108–109.

[28]C. D.Blasi, Progr Energy Combust Sci 19(1993) 71–104.

[29]M. J. Antal, G. Varhegyi, Ind Eng Chem Res 34 (1995) 703–17.

[30]D. L. Pyle, C. A. Zaror, Chem Eng Sci 19(1984) 147–58.

[31]Shafizadeh F. Pyrolytic reactions and products of biomass. In: Overend RP, Milne TA, Mudge LK, editors. Fundamentals of biomass thermochemical conversion. London: Elsevier; 1985.p. 183–217.

[32]F. Shafizadeh, P. P. S. Chin, ACS Symp Ser 43(1977) 57–81.

[33]F. Thurner, U. Mann, Ind Eng Chem Proc Des Dev 20(1981) 482–8.

[34]W. C. Gorton, J. A. Knight, Biotechnol Bioeng Symp 14(1984) 15–20.

[35]B. M. Wagenaar, W. Prins, W. P. M. V. Swaaij, Fuel Proc Technol 36(1994) 291–302.

[36]S. M. Ward, J. Braslaw, Combust Flame 61(1985) 261–9.

[37]G. Varhegyi, M. J. Antal, E. Jakab, P. Szabo, J Anal Appl Pyrol 42(1996) 73–87.

[38]Varhegyi G, Szabo P, Antal M J. Reaction kinetics of the thermal decomposition of cellulose and hemicellulose in biomass materials. In: Bridgwater AV, editor. Advances in thermochemical biomass conversion. London: Blackie Academic & Professional; 1994. p. 760–71.

[39]H. Teng, Y. C. Wei, Ind Eng Chem Res 37(1998) 3806–11.

[40]G. Varhegyi, M. G. Gronli, C. D. Blasi, Ind Eng Chem Res 43(2004) 2356–67.

[41]M. G. Gronli, G. Varhegyi, C. D. Blasi, Ind Eng Chem Res 41(2002) 4201–8.

[42]A. Rostami, J. Murthy, M. Hajaligol, Fuel 83 (2004) 1527–1536.

[43]A. Auedraogo, J. C. Mulligan, J. G. Cleland, Combust. Flame 114 (1998) 1–12.

[44]Y.B. Yang, V.N. Sharifi, J. Swithenbank, Fuel 83 (2004) 1553–1562.

[45]Y.B. Yang, C. Ryu, A. Khor, V. N. Sharifi, J. Swithenbank, Fuel 84 (2005) 2026–2038.

[46]A. Demirbas, Progress in Energy and Combustion Science 30 (2004) 219–230.

[47]A. Galgano, C. D. Blasi, Combust. Flame 139 (2004) 16–27.

[48]http://www.olive.or.jp/shimameshi/2007/04/post_67.html

[49]T.Ida, A.Nakanishi, Osaka TLO, Patent No. 4088933 (2006) Japan.

[50]J.E.G.van Dam, M.J.A.van den Oever, W.Teunissen, E.R.P.Keijsers, A.G.Peralta, Process for production of high density/high performance binderless boards from whole coconut husk Part 1: Lignin as intrinsic thermosetting binder resin, Industrial Crops and Products, Vol.19 (2004) 207–216.

[51]N. Okuda, K. Hori, M. Sato, J. Wood Sci 52 (2006) 244–248.

[52]http://www.gfc.hokudai.ac.jp/iad/service/genso_CHN.html.

[53]E.Kharbat, K.Annamalai, C.Gopalakrishnan, Combust. Flame 100 (1995) 413–421.

[54]J. Collazo, J. Porteiro, D. Patino, E. Granada, Fuel 93(2012) 149-159.

[55]G. Thomas, D. Kim, D. J. Anker, G. Peter, Fuel 82 (2003) 825–833.

[56]C. W. Lautenberger, A generalized pyrolysis model for combustion solids, Ph.D. thesis, University of California, Berkeley, U.S., 2007.

[57]A. F. Mills. Mass Transfer, Prentice Hall, Upper Saddle River, U.S., 2001, p.161.

[58]D. D. Evans, H. W. Emmons, Fire Safety Journal 1(1977) 57–66.

[59]C. R. Monson, G. J. Germane, A. U. Blackham, L. D. Smoot, Combust. Flame 100 (1995) 669–683.

[60]F. Yi, J. R. Fan, D. Li, S. Q. Lu, K. Luo, Fuel. 90 (2011) 1522–1528.

[61]H.Sutcu, J. Chem. Eng 24(2007) 736–741.

[62]A. W. Coats, J. P.Redfern, Nature 201(1964) 68–69.

[63]H. X. Chen, W. T. Zhao, N. A. Liu, Energy Fuels 25(2011) 797–803.

[64]G. M. Simmons, M. Gentry, J. Anal. Appl. Pyrolysis 10(1986), 129–38.

[65]C. Lautenberger, C. F. Pello, Combust. Flame 156 (2009) 1503–1513.

[66]C. Lautenberger, C. F. Pello, Fire Safety Journal 44(2009) 819–839.

Appendix

```
PROGRAM TEMPERATURE
IMPLICIT NONE
REAL(8) :: Mb0,HIGH,Db,AREAb,DEN0,Cb,Lb0,Cbdry,Cpm,Cpchar,Lbdry,Lm,Lchar
REAL(8) :: dt,t0,dX,X0,dV,dM0,aaa,bbb,ccc,ddd,eee,fff,mmm,nnn,kkk,III,ppp
REAL(8):: R,Av,Ev,Qv,DENco,DENco2,DENch4,DENh2,Cme,Yini,Deini, Cair,SHG,Kc,Re,Nu,Ad,H1,Qg,Ql,Qm,Dn
REAL(8) :: Aw,Ew,Cw,Qw,DENw,Lw,dMmois0
REAL(8) :: Ac,Ec,Qc,Fabs,F,DZ,Ts,Tse,Tr,Lc0,ARFA,RATIO,FCO2
REAL(8) :: MWBIC0,MDBIC0,MC0,MA0,DMWBIC0,DMDBIC0,DMC0,DMA0,MW0,MV0,DMW0,DMV0,DDEN0,DMBO,DMBIC0
REAL(8) :: TEMPa,La,Ua,Na,PRa,H,No,Dena,VF
REAL(8) :: M0,M,Mvg,Mwg,Vvg,Vwg,Uv,Uw,Xco2,Xh2o
REAL(8) :: U,GCw,GCf,Lg,SIG,Kf,Qr,Q
REAL(8) :: aa,bb,cc,dd,ee,TIME,FACE,TEMP10,TEMP20,TEMP30
REAL(8) :: Umin,Qf,Z,TEMPf,Yo
REAL(8) :: CONV,COND,RADI,HEATG,ENCH
REAL(8) :: TCT,TCB,AP0,AP,AB,AT,TSOLD
REAL(8) :: DENO2,WO2,AO2,SIGMAO2,EPSKO2,DENN2,WN2,SIGMAN2,EPSKN2,SHHO2,SHHN2,TST,OMEGA,VISHO2,VISHN2,
          TCHO2,TCHN2,DIFHAIR,HM,NA1
INTEGER :: x,t,nn,KK,LL,MM,WFRONT,VFRONT
INTEGER,PARAMETER :: I=3000
INTEGER,PARAMETER :: J=1800000
REAL(8),DIMENSION(I) :: TEMP,Xb,Ls,dMmois,Mfw,Cp,POROSITY,DMWBIC,DMDBIC,DMC,DMA,DMW,DMV,DDEN,DMB,
                        YWBIC, YDBIC, YC, YA, DDENO, LD, DMCA
REAL(8),DIMENSION(I) :: Fw,Fv,Fc,Fcg,SHWBIC,SHDBIC,SHASH,SHCHAR,TCWBIC,TCDBIC,TCASH,TCCHAR
REAL(8),DIMENSION(J) :: M1,Uv1,Vw1,U1,TIME1,TEMPf1,Z1,Q1
REAL(8),DIMENSION(10000) :: FACE1,TIME2,TEMP101,TEMP201,TEMP301
REAL(8),DIMENSION(10000,I) :: TEMP1,dM1,Fw1,Fv1,Ls1,Cp1,POROSITY1
REAL(8),DIMENSION(10000) :: Ts1,CONV1,COND1,RADI1,HEATG1
REAL(8),DIMENSION(10000) :: LsOLD,DENS,DENSOLD,CPOLD,MDOT,MDOTOLD,QSG,QVOR,TEMPOLD,QSGOLD,MDOTW,
                            MDOTV
!*****************BIC PROPERTY*******************************
Mb0=0.212                                   ! MASS OF BIC (kg)
HIGH=9d-2                                   ! LENTH OF BIC(m)
Db=4.8d-2                                   ! DIAMETER OF BIC (m)
AREAb=(Db**2)*3.14/4                        ! AREA OF BIC END SURFACE (m2)
DEN0=Mb0/(AREAb*HIGH)                       ! BIC INITIAL DENSITY(kg/m3)
dX=3d-5
DV=AREAb*dX                                 !GRID DISTANCE(m)
III=HIGH/dX
MWBIC0=(1-0.07)*Mb0
MDBIC0=0
MC0=0
MA0=0.07*Mb0
MW0=Mb0*0.1
Mv0=Mb0*0.7
```

```
DMBO=Mb0/III
DMWBIC0=MWBIC0/III
DMDBIC0=MDBIC0/III
DMC0=MC0/III
DMA0=MA0/III
DMW0=MW0/III
DMV0=MV0/III
DDEN0=DEN0
!******************TIME PARAMETER AND GRID******************
dt=1d-3                                  !TIME STEP (s)
t0=dt*J/60                               !TIME STEP (min)
!******************WATER DRYING PARAMETER******************
Aw=5.13d6                                !MOISTURE PRE FREQUENCE FACETOR    (1/s)
Ew=107672.775                            !MOISTURE ACTIVATION ENERGY (J/mol)
Qw=-2.5d6                                !WATER DRYING ENGERGY (J/kg)
DENw=18/22.4                             !WATER VAPOR DENSITY (kg/m3)
WFRONT=0
!******************PYROLYSIS REACTION**********************
Av=3731.628453                           !VOLATILE PRE FREQUENCE FACETOR    (1/s)3731.628453
Ev=73403.7318                            !VOLATILE ACTIVATION ENERGY (J/mol)
DENco=28/22.4                            !CO DENSITY (kg/m3)
DENco2=1.797                             !CO2 DENSITY (kg/m3)
DENch4=16/22.4                           !CH4 DENSITY (kg/m3)
DENh2=2/22.4                             !H2 DENSITY (kg/m3)
Qv=-2.5d5                                !PYROLYSIS REACTION HEAT (J/kg)
VFRONT=0
!******************CHAR OXIDATIVE REACTION******************
Ac=1.2d3                                 !CHAR OXIDATIVE PRE FREQUENCE FACETOR (m/s)
Ec=8.38d4                                !CHAR OXIDATIVE ACTIVATION ENERGY (J/mol)     8.38
Qc=3.3d7                                 !CHAR OXIDATIVE REACTION HEAT (J/kg)
Tr=273                                   !REFERENCE TEMPERATURE(K)
!******************CONSTANT GAS PARAMETER*******************
R=8.31                                   ! (J/K*mol)
!******************HOT AIR******************
DENO2     = 1.301
WO2       = 32.0
SIGMAO2 = 3.467
EPSKO2    = 106.7
DENN2     = 1.138
WN2       = 28.0
SIGMAN2 = 3.798
EPSKN2    = 71.4
Yini=0.21                                !AIR OXYGEN MASS FRACTION
Deini=0.21*DENO2+0.79*DENN2              !AIR DENSITY WHEN TEMPERATURE IS 273K(kg/m3)
TEMPa=873                                !HOT AIR TEMPERATURE(K) change
PRa=0.8                                  !PRANTL NUMBER (-)
VF=550                                   !HOT AIR FLUX
```

```
Dn=0.05                                    !NOZZLE DIAMETER(m)
SHHO2 = 9.26844E2+1.91789E-1*TEMPa-3.70788E-5*(TEMPa**2)+2.99313E-9*(TEMPa**3)-6.86447E6*(TEMPa**(-2))
SHHN2 = 9.31857E2+2.93529E-1*TEMPa-7.05765E-5*(TEMPa**2)+5.68836E-9*(TEMPa**3)+1.589693E6*(TEMPa**(-2))
Cair   = 0.21*SHHO2+0.79*SHHN2
TST        = TEMPa/EPSKO2
OMEGA     = 1.16145*(TST**(-0.14874))+0.52487*EXP(-0.77320*TST)+2.16178*EXP(-2.43787*TST)
VISHO2    = 26.69E-7*(WO2*TEMPa)**0.5/(SIGMAO2**2*OMEGA)
TCHO2     = VISHO2*SHHO2/PRa
TST        = TEMPa/EPSKN2
OMEGA     = 1.16145*(TST**(-0.14874))+0.52487*EXP(-0.77320*TST)+2.16178*EXP(-2.43787*TST)
VISHN2    = 26.69E-7*(WN2*TEMPa)**0.5/(SIGMAN2**2*OMEGA)
TCHN2     = VISHN2*SHHN2/PRa
La          = 0.21*TCHO2+0.79*TCHN2
Na          = 0.21*VISHO2+0.79*VISHN2
Ua          =VF*TEMPa/(1000*60*3.14*0.024*0.024*298)     !HOT AIR VELOCITY (m/s)
Dena       =Deini*298/TEMPa                !HOT AIR DENSITY(kg/m3)
DIFHAIR=La/Cair/Dena
RE         =Dena*Ua*DN/Na                  !REYNILDS NUMBER
NU         =0.661*(RE**0.566)/(2.2**0.078)
H          =NU*La/Db                       !HEAT TRANSFER COEFFICIENT (W/m2*K)
HM         =NU*DIFHAIR/Db                  !MASS TRANSFER COEFFICIENT
SIG                    =5.67D-8            !boltzman constant (w/m2*k4)

OPEN (UNIT=1,FILE='TEMPERATURE.TXT',FORM='FORMATTED',STATUS='UNKNOWN')
OPEN (UNIT=2,FILE='MASS.TXT',FORM='FORMATTED',STATUS='UNKNOWN')
OPEN (UNIT=3,FILE='GASFLOW.TXT',FORM='FORMATTED',STATUS='UNKNOWN')
OPEN (UNIT=4,FILE='EDGE_POSITION.TXT',FORM='FORMATTED',STATUS='UNKNOWN')
OPEN (UNIT=5,FILE='SURFACE_TEMP.TXT',FORM='FORMATTED',STATUS='UNKNOWN')
OPEN (UNIT=6,FILE='HEAT_TRANSFER.TXT',FORM='FORMATTED',STATUS='UNKNOWN')
OPEN (UNIT=7,FILE='REMAIN.TXT',FORM='FORMATTED',STATUS='UNKNOWN')
OPEN (UNIT=8,FILE='WREACTION_RATE.TXT',FORM='FORMATTED',STATUS='UNKNOWN')
OPEN (UNIT=9,FILE='VREACTION_RATE.TXT',FORM='FORMATTED',STATUS='UNKNOWN')
OPEN (UNIT=10,FILE='THERMAL_CONDUCTIVITY.TXT',FORM='FORMATTED',STATUS='UNKNOWN')
OPEN (UNIT=30,FILE='THERMAL_CAPACITY.TXT',FORM='FORMATTED',STATUS='UNKNOWN')
CLOSE (UNIT=1)
CLOSE (UNIT=2)
CLOSE (UNIT=3)
CLOSE (UNIT=4)
CLOSE (UNIT=5)
CLOSE (UNIT=6)
CLOSE (UNIT=7)
CLOSE (UNIT=8)
CLOSE (UNIT=9)
CLOSE (UNIT=10)
CLOSE (UNIT=30)
STOP
END PROGRAM TEMPERATURE
```

Achievements

Journal publications:

1. **H. Yan**, O. Fujita, "Study of the transient combustion of highly densified biomass briquette (Bio-coke) in an air flow", *Fuel* 188 (2017) 595–602.
2. T. Nakahara, **H. Yan**, H. Ito, O. Fujita, "Study on one-dimensional steady combustion of highly densified biomass briquette (bio-coke) in air flow", *Proceedings of the Combustion Institute* 35 (2015) 2415–2422.

Conference publications:

1. **H. Yan**, O. Fujita, "Study of the transient combustion of highly densified biomass briquette (Bio-coke) in an air flow", *36th International Symposium on Combustion*, Seoul, Korea, (2016. 8, Poster presentation).
2. **H. Yan**, O. Fujita, "Verification of the Absence of Combustion Processes in the Tobacco Heating System", *21st International Symposium on Analytical and Applied Pyrolysis*, Nancy, France, (2016. 5, Poster presentation).
3. **H. Yan**, O. Fujita, "Numerical calculation on transient combustion of Bio-coke in convective air flow", *52nd Symposium (Japanese) on Combustion*, Okayama, Japan, (2014. 12, Oral presentation).
4. T. Nakahara, **H. Yan**, H. Ito, O. Fujita, "Study on one-dimensional steady combustion of highly densified biomass briquette (bio-coke) in air flow", *35th International Symposium on Combustion*, San Francisco, USA, (2014. 8, Oral presentation).
5. **H. Yan**, O. Fujita, "Numerical calculation on transient combustion of Bio-coke in convective air flow", *Proc. 51st Japanese heat transfer Symp*, Hamamatsu, Japan (2014.

5, Oral presentation).

6. **H. Yan**, T. Nakahara, H. Ito, O. Fujita, "Numerical calculation on extinction limit of Bio-coke in convective air flow", *The 3rd East Asia Mechanical and Aerospace Engineering Workshop* Sapporo, Japan (2013. 6, Poster presentation).
7. **H. Yan**, O. Fujita, "Numerical calculation on extinction limit of Bio-coke in convective air flow", *9th Asia–Pacific Conference on Combustion*, Gyeongju, Korea (2013. 5, Oral presentation).
8. **H. Yan**, O. Fujita, "Numerical simulation on extinction criterion of Bio-coke in convective air flow", *50th Symposium (Japanese) on Combustion*, Nagoya, Japan, (2012. 11, Poster presentation).
9. **H. Yan**, T. Nakahara, H. Ito, O. Fujita, "Numerical calculation on extinction limit of Bio-coke in convective air flow", *The 8th HU-SNU Joint Symposium*, Sapporo, Japan (2012. 8, Poster presentation).

Awards:

1. "**Young Researcher Award**", *9th Asia Pacific Conference on Combustion*, Gyeongju, Korea. 2013. 5
2. Selected as scholarship student supported from China Scholarship Council, China (2010. 10).
3. Selected as a scholarship student from JASSO Honors Scholarship of Hokkaido University, Japan (2014. 4).